NUREG-1781

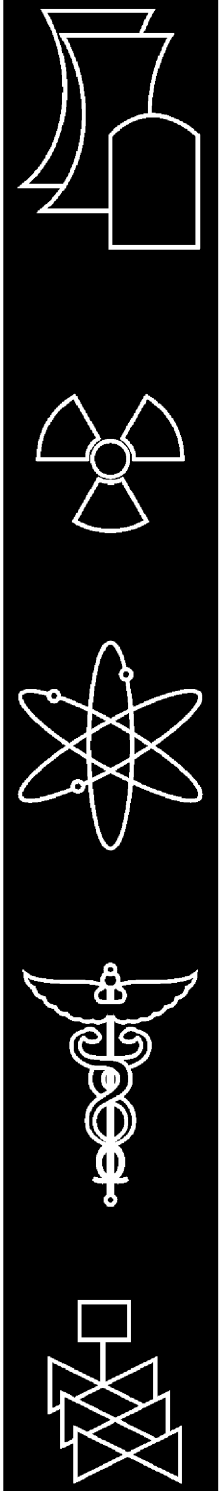

CFD Analysis of 1/7th Scale Steam Generator Inlet Plenum Mixing During a PWR Severe Accident

U.S. Nuclear Regulatory Commission
Office of Nuclear Regulatory Research
Washington, DC 20555-0001

NUREG-1781

CFD Analysis of 1/7th Scale Steam Generator Inlet Plenum Mixing During a PWR Severe Accident

Manuscript Completed: September 2003
Date Published: October 2003

Prepared by
C.F. Boyd, K. Hardesty

Division of Systems Analysis and Regulatory Effectiveness
Office of Nuclear Regulatory Research
U.S. Nuclear Regulatory Commission
Washington, DC 20555-0001

ABSTRACT

Computational fluid dynamics (CFD) is used to predict steam generator inlet plenum mixing during a severe accident scenario in a pressurized water reactor. Comparisons are made to 1/7th scale data. Qualitatively, the code predicts the experimental flow patterns and mixing phenomena. Quantitatively, comparisons are made with key temperatures, mass flows, and mixing parameters. The best estimate prediction is generally within 5% of the reported values. Key temperature predictions are within a few degrees K of the test data. Boundary conditions applied to the model include the hot leg inlet mass flow and temperature as well as the tube secondary side temperature and heat transfer. The mass averaged temperature of the flow entering the tubes is predicted to within 1 degree of the experimental data. The mass flow through the tube bundle is predicted to within 0.5% of the data. The number of hot tubes is overpredicted by 7 tubes out of the 216 total. The mixing fraction and the recirculation ratio, both important mixing parameters, are predicted to within 5% of the data. These predictions provide confidence in the code and modeling approach. The secondary side heat transfer coefficient is determined to be the dominant governing parameter.

CONTENTS

Page

Abstract iii

Executive Summary ix

Foreword xi

1 Introduction 1

2 Computational Fluid Dynamics (CFD) 3

3 Physical Model Description 5

3.1 Hot Leg 5

3.2 Inlet and Outlet Plenum 6

3.3 Steam Generator Tubes 6

3.4 Steady State Test Description 6

3.5 Scaling Parameters 6

4 CFD Model Development 9

4.1 Finite Volume Mesh 9

4.2 Boundary Conditions 9

4.2.1 Tube Model 10

4.2.2 Velocity Inlet Conditions 10

4.3 Material Properties 11

4.4 Turbulence Modeling 11

4.5 Solution Convergence 11

4.6 Grid Independence 11

5 Completed Predictions 13

5.1 Summary of Assumptions and Limitations 13

6 Results 15

6.1 Best Estimate Results 15

6.2 Hot Leg Prediction 18

6.3 Nozzle Region Predictions 18

6.4 Inlet Plenum Flows 19

CONTENTS (continued)

Page

6.5 Tube Bundle Flows 19
6.6 Sensitivity Study Results 20
6.6.1 Inlet Temperature Sensitivity 21
6.6.2 Hot Leg Inlet Mass Flow (Inlet Velocity) Sensitivity 21
6.6.3 Turbulence Model Sensitivity 22
6.6.4 Tube Sheet Entrance Pressure Loss Sensitivity 22
6.6.5 Tube Flow Viscous Loss Sensitivity 23
6.6.6 Tube Heat Transfer Coefficient Sensitivity 23
7 Summary 25
8 References 27

Appendix

A Appendix A A-1

Figures

1. Overview of Natural Circulation Flow Pattern 28
2. Cross Section of Inlet Plenum, Hot Leg, and Tube Sheet 28
3. Computational Mesh 29
4. Boundary Between Hot and Cold Tubes 29
5. Hot Leg Temperature Prediction and Data (x = -0.566 m) 29
6. Hot Leg Temperature Contours and Velocity Profiles 30
7. Path Lines on Symmetry Plane of Inlet Plenum 30
8. Contours of Turbulence Intensity on Symmetry Plane of Inlet Plenum 31
9. Normalized Temperature Contours on Symmetry Plane of Inlet Plenum 31
10. Velocity Vectors on Vertical Planes Normal to Symmetry Plane 32
11. Temperature Contours on Horizontal Planes in Inlet Plenum 33

CONTENTS (continued)

Page

12. Temperature Contours on Vertical Planes Parallel to Symmetry Plane 34
13. Temperature Contours on Horizontal Plane 1 Inch Above Tube Sheet Entrance . 35
14. Histogram of Normalized Hot Temperatures 1 Inch Above Tube Sheet Entrance . 35
15. Predicted Temperature Contours on Model Symmetry Plane 36

Tables

1. SF_6 Properties (2.07 MPa, 300 psia) 37
2. Summary of Boundary Conditions 37
3. Assumptions and Limitations 38
4. Comparison of Test Data (SG-S3) with FLUENT Predictions 39
5. Boundary Conditions for Sensitivity Studies 40
6. Summary of Sensitivity Study Results 41

EXECUTIVE SUMMARY

This report describes the first step in a new analysis of steam generator inlet plenum mixing using computational fluid dynamics (CFD).

Inlet plenum mixing is one of the important parameters governing the degree of thermal challenge to steam generator tubes during postulated severe accidents in pressurized-water reactors (PWRs). The NRC has implemented a steam generator action plan to confirm the robustness of risk-informed licensing decisions and to reduce modeling uncertainties and improve the technical basis for future licensing requests. One objective of this plan is to investigate the time-dependent thermal-hydraulic conditions in the hot leg and steam generator. This research will ultimately lead to a reduction in the uncertainties in modeling these conditions. One aspect of this research involves using state-of-the-art CFD techniques to predict inlet plenum mixing. The first step in this process is to evaluate the modeling technique using existing experimental data at 1/7th scale.

There are two significant benefits from comparing computed predictions with experimental data. First, the applicability of the modeling technique is established through a comparison with the test data. This provides a level of confidence in the modeling approach, which will ultimately be applied to full-scale steam generators under a variety of conditions not explicitly covered by the available tests. The second benefit from these predictions is clarifying specific aspects of the experimental data. The 1/7th scale data serve as a primary source of information about the thermal-hydraulic conditions in the hot leg and steam generator during severe accident natural circulation conditions. The data, however, consist only of thermocouple measurements at a limited number of locations. Details of the mixing behavior are not available. The CFD predictions provide three-dimensional results for velocity, temperature, turbulence, and other flow parameters over the entire domain of the hot leg and inlet plenum. These predictions provide insights into the flow and mixing behavior that were previously unavailable from the limited experimental measurements.

A best estimate analysis is completed using boundary conditions derived from a specific test (SG-S3) at 1/7th scale. A high-quality computational mesh is developed that represents the key features of the test facility. The FLUENT 6.0 CFD code is used for the analysis. Qualitatively, the predictions show all of the experimentally observed flow features in the hot leg and steam generator regions. Predicted features such as the sloping interface in the hot leg, the relative sizes of the hot and cold flow regions, and the path and size of the inlet plenum plume are consistent with the experimental observations. The global natural circulation flow pattern is also well predicted by the CFD code.

The test data indicate a significant temperature reduction between the locations of the last hot leg thermocouple and the first set of inlet plenum thermocouples encountered by the hot plume. This temperature reduction occurs as the flow travels through the nozzle region of the hot leg, where no measurements are available and the flow pattern is unknown. The predictions also indicate a significant amount of mixing in this region. The specific flow pattern responsible for this significant mixing is clearly evident in the CFD predictions. Cold flow returning to the hot leg from the inlet plenum intersects the hot stream exiting the hot leg, resulting in significant mixing at this location. This result results in a better understanding of the experimental result.

The key mixing parameters predicted are generally within 5% of the measured values. Key temperature predictions are typically within a few degrees of the experimental data. The most significant predicted values are associated with the tube bundle temperatures and mass flows. These predictions essentially match the test data. The predicted average temperature entering the tube bundle is within 1 degree Kelvin of the reported test result. The tube bundle mass flow prediction is within 0.5% of the experimental value. The ability to predict these two key parameters establishes confidence in the modeling technique. The predicted shape and location of the hot tube region match the data. Seven more tubes (out of 216 tubes in the bundle) are predicted to carry hot flow than were observed experimentally.

One benefit of the CFD predictions is the ability to determine tube-to-tube variations. The data include tube entrance temperatures for 25% of the tube bundle, providing a limited indication of the tube-to-tube variation. The 3 dimensional predictions for temperatures and mass flows provide a complete description of the tube-to-tube variations and provide a means to fill in the gaps where no data exists.

A series of sensitivity studies are completed to establish the stability of the model and the impact of major modeling assumptions. Key input parameters are systematically varied to determine the governing phenomena. The secondary side heat transfer coefficient is determined to be the dominant governing parameter with respect to the key mixing parameters. The variations observed also explain a key feature of the data at $1/7^{th}$ scale that has raised questions in previous investigations. Specifically, the data result in significant variations in the mixing parameters between the steady state and transient tests. The sensitivity studies indicate that these differences are due to the differences in the secondary side heat transfer rate. This finding helps to focus the efforts to reduce the uncertainty associated with the prediction of severe accident natural circulation phenomena.

These results demonstrate the applicability of the CFD technique for this type of analysis and provide detailed insights into the existing data. The results are a first step towards the goal of completing CFD analysis of full-scale steam generators under a variety of conditions not specifically addressed by the test data. These conditions include the effect of tube leakage and the effect of geometrical differences in inlet plenum geometry. The predictions at $1/7^{th}$ scale are a necessary step. The agreement with the test data provides confidence in the modeling approach and assumptions that will be used at full-scale conditions.

FOREWORD

Steam generator tube integrity during severe accidents is a critical safety issue. Tube failure during these accidents results in a containment bypass with the associated radioactive release to the environment. Alternatively, failures of other reactor coolant system (RCS) components prior to the tube failure leads to a depressurization of the RCS and an elimination of the threat to the tubes. Existing predictions indicate that the time for RCS failure at locations such as the hot leg or surge line connection is very close to the predicted time of tube failure. It is necessary to identify and reduce uncertainties in these predictions to improve the agency's ability to assess the likelihood of steam generator tube failures during severe accidents.

Thermal-hydraulic analysis of the RCS provides the temperature and pressure conditions that challenge the RCS components and the steam generator tubes. Temperature of the steam in the tubes is influenced significantly by three-dimensional mixing behavior in the steam generator inlet plenum region. System codes such as SCDAP/RELAP5 do not implicitly model this mixing. Mixing coefficients are pre-determined based mainly on a limited set of experiments at $1/7^{th}$ scale. The experimental data provide valuable information but are limited in scale and range of application. For instance, the effects of tube leakage and inlet plenum geometry variations on the inlet plenum mixing cannot be assessed from the experiments. The Office of Research (RES) has been using state-of-the-art computational fluid dynamics (CFD) to study a variety of safety issues. CFD provides a tool for predicting the steam generator inlet plenum mixing under a wide variety of conditions. The first step in the application of CFD to the steam generator inlet plenum mixing issue is an assessment of the tool against the existing $1/7^{th}$ scale data.

This report describes the completion of a detailed analysis of steam generator inlet plenum mixing at $1/7^{th}$ scale using CFD. The goal is to confirm the applicability of CFD for this type of analysis and to enhance the NRC's understanding of the phenomena governing steam generator inlet plenum mixing. The analysis supports the NRR user need request related to steam generator severe accident response dated September 7, 2000. This request and subsequent related issues are incorporated into the agency's Steam Generator Action Plan (memorandum from Samuel Collins and Ashok Thadani to William Travers, May 11, 2001). The steam generator action plan is intended to confirm the robustness of risk-informed licensing decisions and to reduce modeling uncertainties and improve the technical basis for future licensing requests.

The successful completion of this work represents an important milestone in the thermal-hydraulic analysis of the RCS. The predictions agree well with the experimental results and the applicability of the method for this type of analysis is established. This results provide a level of confidence in the succeeding full-scale predictions under a variety of conditions (The full-scale work is being documented separately). In addition, the understanding of the $1/7^{th}$ scale data has significantly improved due to the detailed predictions of the mixing phenomena in regions where no data are available. Assumptions and limitations of this analysis are outlined in Table 3.

Farouk Eltawila, Director
Division of Systems Analysis and Regulatory Effectiveness
Office of Nuclear Regulatory Research

1 INTRODUCTION

The Nuclear Regulatory Commission (NRC) has implemented a steam generator action plan[1] to address tube integrity issues. This plan includes tasks to predict steam generator inlet plenum mixing during a severe accident scenario using computational fluid dynamics (CFD). The sequence of interest in this study is a station blackout that leads to a loss of secondary side cooling and a loss of primary inventory. As the core is uncovered, natural circulation of superheated steam carries heat to structures, including the upper reactor vessel, hot leg, and steam generator tubes. In the scenario considered, the loop seals are filled with water and full loop circulation is blocked. A countercurrent natural circulation flow pattern, as illustrated in Figure 1, is expected during this phase of the accident.

This scenario leads to a failure in the primary coolant loop. The thermal-hydraulic details determine whether this failure occurs in the reactor coolant piping (within containment) or in the steam generator tubing (with a leak path to the outside of containment). Steam generator inlet plenum flow and mixing phenomena play a significant role in determining the temperature of the steam that enters the tubes. A lack of mixing allows high temperature steam to enter the tubes and consequently reduces the time before tube failure. Significant inlet plenum mixing reduces the temperature of the hot steam entering the tubes. This increases the time before tube failure, making it more likely that some other component in the system will fail first. If another component fails (e.g., the surge line), the system will depressurize into the containment and the threat to the tubes will be eliminated. A tube rupture represents a bypass of containment and a potential radioactive release to the environment. Therefore, it is important to accurately predict when the tubes (and other components) are expected to fail. Inlet plenum mixing is one parameter needed for this prediction. Background information on many aspects of severe accident-induced steam generator tube rupture can be found in NUREG/CR-6285[2] and NUREG-1570.[3]

The thermal-hydraulic modeling of this severe accident scenario is typically performed with lumped parameter codes such as SCDAP/RELAP5 or MELCOR. The efficiency gained by the coarse nodilization of this approach makes it feasible to predict the transient behavior of the entire reactor coolant system over extended periods of time. A limitation of these models is a reliance on predetermined flow-field and mixing parameters to address any 3 dimensional flow phenomena including the steam generator inlet plenum flows during the countercurrent natural circulation phase of the transient. The primary source of data for the inlet plenum mixing parameters during this type of natural circulation flow comes from experiments in a Westinghouse 1/7th scale test facility.[4]

The NRC is interested in mixing parameters under a variety of full-scale conditions not explicitly covered in the experimental tests. Full-scale experiments are not practical. The NRC plans to use CFD to predict mixing parameters at conditions not explicitly covered by the experiments. First, the applicability of the technique will be established using the 1/7th scale test data. This initial evaluation is the subject of this report. With confidence established in the technique at 1/7th scale, full-scale simulations under a variety of conditions will be evaluated in future work.

2 COMPUTATIONAL FLUID DYNAMICS (CFD)

The FLUENT (version 6.0) CFD code is used to predict the inlet plenum mixing and the natural circulation flows. FLUENT is a commercially available, general-purpose CFD code capable of solving a wide variety of fluid flow and heat transfer problems. The code solves the Reynolds-averaged Navier-Stokes equations on a finite volume mesh. The Navier-Stokes equations represent the mass, momentum, and energy conservation equations for a continuous fluid. Reynolds averaging creates the need for turbulence modeling to account for the turbulent diffusion of momentum and energy. The FLUENT code provides several turbulence modeling options. Unstructured meshing capabilities allow the code to be applied to complex geometries. Commercial CFD codes such as FLUENT are widely used in many industries today and are commonly used to predict mixing phenomena.

Each of the steps in a CFD analysis can influence the predicted results and should be considered. The basic steps involve describing the physical model; defining the CFD model domain, boundary conditions, and models; validating the solution; and completing sensitivity studies. When considering CFD predictions, the analyst must consider the assumptions and limitations of each step in the process. Further details on the fundamentals of CFD are found in the introductory text by Anderson.[5]

3 PHYSICAL MODEL DESCRIPTION

The physical model description is based upon a Westinghouse 1/7th scale test facility.[4] This facility is designed to study the natural circulation phenomena during the severe accident scenario illustrated in Figure 1. The outlet pipe from the steam generators, the loop seal, and the cold legs are not included in the test facility since they do not participate in this scenario. Sulfur hexafluoride (SF_6) is used as the working fluid to make the scale of the facility closer to the prototype.

The 1/7th scale facility is based upon the Indian Point 2 nuclear power plant, which has a Westinghouse model 44 steam generator. However, the steam generator of the 1/7th scale facility does not have full geometric similarity with the prototype. For example, the scaled facility has a total of 216 tubes to represent the 3260 tubes of a full-scale model 44 steam generator. In addition, the orientation of the hot leg relative to the inlet plenum is different. The 1/7th scale facility has a hot leg oriented in a vertical plane normal to the divider plate that separates the inlet and outlet plenums. This orientation of the hot leg makes the steam generator symmetric. The hot leg nozzle of the model 44 steam generator, on the other hand, is oriented approximately 30 degrees from a vertical plane normal to the divider plate. This design does not have a symmetry plane. The effect of geometric variations will be studied in future work. Scaling arguments and background for the 1/7th scale facility are given in Reference 3.

The Westinghouse 1/7th scale facility simulates the primary system of interest for one-half of a four-loop Westinghouse pressurized water reactor (PWR). The reactor vessel is cut in half and attached to two hot legs that lead to a right and left steam generator. Electrical heating provides the power to the core. The entire system is insulated. Cooling water around the upper vessel and the steam generator tubes provides the only significant heat removal during the steady state tests. A diagram of the hot legs, inlet plenum, and the start of the tube bundle is given in Figure 2 for the left steam generator. A coordinate system is attached to the steam generator to help define the model (see Fig. 2). The origin is centered on the tube sheet face. The y-axis points up and is parallel to the tubes. The x-axis, which is parallel to the hot leg axis, points away from the vessel. The z-axis is obtained from the right hand rule. A CFD model is created for one hot leg and steam generator. Components included in the model are briefly described below to provide some detail of the features that impact the current study.

3.1 Hot Leg

The hot legs are 0.10226 m (4.026 in.) inner diameter pipes with a 0.762 m (30 in.) centerline length from the exit of the vessel upper plenum to the entrance of the steam generator inlet plenums. The end of the pipe has a 45-degree radius elbow prior to entering the steam generator. The length of this elbow is 0.127 m (5 in.) on the centerline.

This hot leg is instrumented in three areas as noted by the small black dots on Figure 2. Four thermocouples are positioned on the vertical centerline near the entrance and exit to the hot leg. Each thermocouple is reported to be at the centroid of a section that represents one-fourth of the total pipe flow area. Near the center of the hot leg, six thermocouples are positioned on a vertical centerline. These thermocouples are spaced 0.00635 m (0.25 in.) apart, with three above and three below the horizontal centerline. Due to a limited data system capacity, all of the hot leg thermocouples are not recorded for the test considered in this report.

3.2 Inlet and Outlet Plenum

The inlet and outlet plenums are also shown in Figure 2. Each plenum consists of a 0.2413 m (9.5 in.) inner radius hemisphere attached to a 0.04115 m (1.62 in.) long vertical cylindrical section that attaches the lower hemisphere to the tube sheet. The center point of the hemispherical section is 0.04115 m (1.62 in.) below the tube sheet face. The plenum outer wall thickness is 0.0127 m (0.5 in.). Furthermore, a 0.0127 m (0.5 in.) divider plate separates the inlet and outlet plenums. The tube sheet forms the upper boundary of the inlet and outlet plenum.

3.3 Steam Generator Tubes

The test facility tube bundle consists of 216 U-shaped tubes with a 0.007747 m (0.305 in.) inner diameter and a 0.009525 m (0.375 in.) outer diameter. They are anchored into a 0.1143 m (4.5 in.) thick tube sheet that caps off the inlet and outlet plenums. The tubes are arranged in a 0.02064 m (0.8125 in.) triangular pitch array. The average tube length is 2.499 m (98.403 in.) and the overall bundle height is 1.124 m (56.06 in.) from the bottom face of the tube sheet. The average U-bend radius is 0.1014 m (3.994 in.).

Nearly one-fourth of the tubes, 51, are instrumented with a thermocouple positioned either 0.0254 m or 0.127 m (1 in. or 5 in., respectively) from the tube entrance. These thermocouples are used to determine whether the tube carries hot or cold fluid.

3.4 Steady State Test Description

A single steady state test, referred to as test SG-S3, is used to evaluate the performance of the CFD model. These data are assumed to represent a snapshot of the quasi-steady transient behavior. During steady state testing, a steady power is applied to the core. Continuous water cooling of the vessel upper plenum and the steam generator tubes removes the core power. The hot leg and steam generator plenums are completely insulated and assumed adiabatic. For the purposes of this study, the scaled reactor vessel provides a steady flow of heated SF_6 into the hot leg and receives the returning cooled SF_6 from the steam generator. Only the hot leg and steam generator are considered. The steam generator tube bundle is covered with a steel cylinder and cooling water is pumped past the outside of the tubes to provide the heat removal capacity. The mass flow rate and temperature rise of the cooling water is measured and used to determine the amount of power leaving the tube bundle. This power, along with available average flow temperature measurements, is used to obtain the hot leg and tube bundle mass flow rates. The tests are run continuously until the measured data are steady.

3.5 Scaling Parameters

The test series utilized a heavy gas, sulfur hexaflouride (SF_6), to increase certain scale parameters to improve the representation of full-scale behavior. SF_6 has a density near 100 kg/m^3 at the test conditions. Two important parameters are noted below. For test SG-S3, the Reynolds number in the hot leg, based upon the hot stream velocity and pipe radius, is over 6×10^4. At full-scale conditions, the Reynolds number is in the range of 10^5. The Grashof number, a measure of the effect of buoyancy on the hot plume in the inlet plenum, is 8×10^{11} in the test facility and estimated at 5×10^{12} for full-scale conditions. The Richardson number, a measure of the ratio of the buoyancy to inertial forces on the plume, is approximately 2×10^2 for both the

1/7th scale data and the full-scale conditions. The magnitudes of these important parameters from the 1/7th scale test are at or near the magnitude estimated for the full-scale plant. The 1/7th test is expected to be a good representation of full-scale behavior based on these limited considerations. Other factors, such as thermal radiation and geometric factors, are not considered here. A complete review of the scaling for the Westinghouse 1/7th scale tests is contained in Appendix B and C of NUREG/CR-6285[3].

4 CFD MODEL DEVELOPMENT

The physical geometry and conditions described above are represented on a finite volume mesh on which the governing Navier-Stokes equations are discretized and solved. The model is developed for the FLUENT version 6.0 unstructured CFD code.

To save computer resources, the symmetry of the hot leg and steam generator is utilized. Only half of the physical model is meshed and a vertical symmetry plane is established through the hot leg and steam generator. Due to poor convergence with the steady state solver, a transient solver is applied with steady boundary conditions to obtain a steady solution. The principal features of the CFD model are summarized below:

- transient Reynolds-averaged Navier-Stokes solution with steady boundary conditions
- vertical symmetry plane through hot leg and steam generator
- Reynolds stress turbulence model (2^{nd} order) with nonequilibrium wall functions
- full buoyancy effects on turbulence (as defined in FLUENT code)
- temperature-dependent thermal properties (SF_6 as working fluid) at constant pressure
- gravity
- 500,000+ finite volume cells (hexagonal mesh)
- segregated solver with 2^{nd} order differencing on momentum and energy
- porous media model representing 216 individual steam generator tube flow paths

Significant modeling attributes and assumptions are further described below.

4.1 Finite Volume Mesh

The finite volume mesh, shown in Figure 3, consists of over half a million hexagonal elements. In the bulk of the mesh, the cell aspect ratio is limited to 2 except for the tube bundle. In the tubes, the cell aspect ratio ranged from 1 at the tube sheet to nearly 5 along straight sections of tube. Cell skew is minimized through careful grid spacing and the use of the hexagonal elements. Growth rate between neighboring cells is limited to 20% with few exceptions. The majority of the cells in the hot leg and plenums are of the same approximate dimensions. The hot leg is meshed with 26 cells along a diameter and the inlet plenum contains approximately 60 cells along a radius.

4.2 Boundary Conditions

Boundary conditions are applied at the walls (both internal and external), the inlet, and the outlet. All walls use a no-slip condition for the momentum equations with zero surface roughness. In addition, all walls are adiabatic with the exception of the tube walls above the tube sheet. The vertical midplane of the steam generator and hot leg is modeled as a symmetry plane. The vessel end of the hot leg is split into two faces to facilitate an inflow and outflow boundary. A 60/40 split based on height is used. This ratio comes from experimental observations. The 60% region on top is where hot gas enters the hot leg from the vessel (velocity inlet condition). The lower 40% of the hot leg pipe end provides an exit for the cooled gas returning to the vessel (pressure outlet condition). The boundary conditions of the hot leg and tube bundle are determined based on the experimentally observed energy balance. These conditions are described in more detail below.

4.2.1 Tube Model

Directly modeling the 216 tubes from the Westinghouse 1/7th scale facility is not practical. This approach requires a model with millions of cells. This size model is impractical for simulations on typical computers in the year 2002. Computational mesh requirements are estimated in the range of tens of millions of computational cells for full-scale steam generators with thousands of individual tubes. To reduce the mesh requirements and to facilatate practical solutions, a simplified tube bundle model is developed that maintains the flow and heat transfer characteristics of the actual tube bundle with significantly fewer computational cells.

In the FLUENT model, square tubes with a larger cross section are used to represent the individual tubes of the Westinghouse facility. Individual flow paths and tube heights are preserved. A porous media option is used in the FLUENT model throughout the tube region. This approach provides a set of modeling coefficients (porous model inputs) that are used to preserve pressure loss and heat transfer characteristics of the tubes even though the cross section is not prototypical. The porous media approach and use of square tubes significantly reduce the meshing requirements needed to compute the tube flows. The square tube cross section is easier to mesh with the hexagonal elements. A single cell can be used to accurately define the cross section. A round tube requires many cells to adequately define the shape of the cross section. The porous media approach also eliminates the need to resolve the tube wall boundary layer sheer stresses and the tube sheet flow reduction pressure loss.

The tube model is validated by looking at one individual tube in detail. A prototypical round tube is discretized with nearly one million cells to study the heat transfer and pressure drop characteristics in great detail. The results are used to define the coefficients used in the equivalent square, porous media tube with 4000 cells. The porous coefficients are adjusted in the FLUENT code to ensure the porous tube approximation reproduces the prototypic tube characteristics over a wide range of conditions. This approach does not accurately resolve flow in individual tubes but does provide a realistic upper boundary condition for the inlet (and outlet) plenum where the mixing of interest takes place. The principal attributes of the tube bundle modeled with this approach are the pressure drop at the tube entrance, the flow (viscous) losses within the tubes, the heat losses from the tubes, and the buoyancy driving forces. Tube bundle mass are governed by a balance between the viscous (and inertial) pressure losses and the buoyancy driving force. The inputs to this model are defined to preserve this balance and result in an appropriate tube bundle mass flow. Further details on the tube bundle modeling approach are outlined in Appendix A.

4.2.2 Velocity Inlet Conditions

The velocity inlet covers a region that represents the upper 60% (based upon height) of the vessel end of the hot leg. It is assumed that the flow coming from the reactor vessel is well mixed and at a uniform temperature and velocity. Further details of the velocity and temperature profiles for flow coming from the vessel are unknown. Sensitivity studies indicated that the flows at the inlet plenum end of the hot leg are not significantly affected by changes in the inlet velocity profile at the vessel end of the hot leg. The uniform velocity and temperature boundary conditions applied at the vessel end of the hot leg are considered a reasonable assumption. Specific values for the inlet temperature and velocity are determined to match the reported hot leg temperature and mass flow from the data.

4.3 Material Properties

The working fluid is sulfur hexafluoride (SF_6). Fluid properties are obtained from graphs and tables in Reference 4. Since the steady state tests are conducted at fixed pressure, properties are specified as temperature dependent only. The properties used in the analysis of test SG-S3 are listed in Table 1. The FLUENT code uses linear interpolation on temperature to find the thermal properties from the table.

4.4 Turbulence Modeling

Two turbulence models are used for the results cited in this report. Second order Reynolds stress modeling (RSM) is used for all predictions with the exception of a sensitivity that uses the first order, isotropic RNG k-epsilon model. Detailed experimental data, not available from the Westinghouse tests, are needed to fully validate and justify the selection of the turbulence model. The second order RSM turbulence model is considered to be the most appropriate model available in the FLUENT code. The RSM model does not assume isotropic turbulence like the two-equation k-epsilon type models. Full buoyancy effects on the turbulence model are applied and nonequilibrium wall functions are used. Details of the turbulence models are beyond the scope of this report.

4.5 Solution Convergence

Steady state solutions are obtained using a transient solver with steady boundary conditions. Initially, each case is run using the steady state solver to obtain a rough solution that serves as the initial condition for the transient solver. The transient solver is used until a steady solution is obtained. Solution convergence is monitored in several ways. First, solution residuals are monitored at each time step to ensure they have dropped sufficiently. In addition, several temperatures and velocities are monitored in key areas. These monitored prediction points asymptotically approach steady values as the solution nears convergence. Finally, an overall mass and energy balance is monitored for convergence.

4.6 Grid Independence

A complete grid independence study is not performed due to the physical scale of the model. A high-quality mesh is used for this analysis to minimize any grid affects on the results. In addition, second order differencing is used to reduce numerical diffusion. Qualitative information on grid independence is given below for completeness.

The final grid for this study contains over 500,000 finite volume cells. In the process of constructing the grid, over 15 separate grids were created and tested. The final grid is a compilation of the lessons learned during this process. Grid optimizations include optimized node density for wall functions and verification of grid independence in the tube bank. The final mesh is created using all hexagonal elements with grid stretching and skew minimized. In regions of high gradients or transitions, the cell aspect ratio is kept very close to 1. Mesh size is reduced at the walls to accommodate the wall functions. Transitions away from the walls are limited to growth rates between 5 and 20%.

Although a full grid independence study is not completed, a high degree of confidence in the quality of the mesh is obtained from localized grid studies, from the high-quality mesh, and ultimately from the accurate prediction of the experimental results.

5 COMPLETED PREDICTIONS

Test SG-S3 is selected from the set of 1/7th scale tests. It is one of the higher temperature and power tests available. Initially, a best estimate case is completed to provide a direct comparison of the predictions with the test data. The boundary conditions applied are determined from the data. Next, a set of sensitivity studies is completed on some of the major modeling input assumptions. This is done to establish the sensitivity of the results to variations in some of the input parameters. Sensitivity studies reported here include variations of the hot leg inlet temperature, hot leg mass flow, turbulence model, tubesheet entrance pressure drop, viscous losses in the tube bundle, and tube heat transfer characteristics. The boundary conditions used in the FLUENT model for these predictions are summarized in Table 2.

Additional sensitivity studies on modeling options such as the turbulent wall treatment, buoyancy effects on turbulence, finite differencing schemes, solution algorithms, and mesh quality were also completed. These studies helped to ensure the solution is stable and not unduly affected by simple modeling assumptions. No significant variations were observed for these unreported sensitivity studies. The studies are noted here only to document that they were considered.

Predictions completed in this study focused on the left steam generator from the facility because the reported mixing parameters and other key variables from the test came from this side. Significant asymmetries between the left and right steam generator data make quantitative comparisons of the predictions with the right side data problematic. The asymmetries are probably caused by the 40% difference in the cooling flow rates applied to the left and right steam generators during the steady state testing.

5.1 Summary of Assumptions and Limitations

The completed CFD predictions give valuable insights into the three-dimensional natural circulation flows in the hot leg and the primary side of the steam generator. However, the final results are dependent upon the modeling assumptions and limitations of the approach. To facilitate a better understanding of the predicted results, a partial list of assumptions and limitations is given in Table 3. These limitations should be considered to gain a better understanding of the results.

6 RESULTS

The results of this study demonstrate that the FLUENT code has the potential to predict the natural circulation behavior in the hot leg and steam generator during this type of severe accident scenario. Qualitatively, the code predicts the flow pattern with specific characteristics that are observed from the test series. Quantitatively, predicted key parameters are in good agreement with the data. The best estimate prediction is described in detail followed by a discussion of the sensitivity studies.

6.1 Best Estimate Results

The results include specific data and integral parameters that are compared with the experimental data.[4] Detailed three-dimensional (3D) predictions of variables are also provided to aid in the understanding of the phenomena. The integral features of the predictions are most useful for assessing inputs to 1D system codes that are used to predict plant behavior during this type of transient. Features such as recirculation ratio, mixing fraction, and tube flow fractions are used to set up simplified inlet plenum mixing models. Table 4 shows significant parameters computed from the CFD results, compared to the experimental data for test SG-S3.[4] Generally speaking, these predicted parameters are in good agreement with the experimental results and are generally assumed to fall within the experimental uncertainty. Individual items are discussed below.

Heat Loss at Tubes. Predicted total tube heat loss is 3.7% above the experimentally reported value. Experimental tube bundle heat loss is determined from a secondary side coolant mass flow rate and temperature rise measurements for this coolant. The experimental uncertainty of the temperature and mass flow measurements and of other system heat losses is not available. The CFD code computes the total tube heat loss as an integral of heat flux over the surfaces of each tube. From a 1st law of thermodynamics analysis, the predicted tube inlet and outlet temperatures and the tube bundle mass flow govern this value. The predicted temperature drop in the tube bundle is 35.3K (63.5 ^{o}F). For a given tube bundle mass flow, one degree (K) difference in the temperature drop changes the total tube heat loss prediction by 3%. The 3.7% difference between the prediction and the measured value is considered insignificant in light of the assumed experimental uncertainty.

Hot Tubes vs. # Cold Tubes. Seven additional tubes are predicted to carry hot flow compared to the reported value. This difference is equal to 3.2% of the total number of tubes (216) in the bundle. Figure 4 illustrates the predicted boundary between the hot (upward) flow tubes and the cold return flow tubes on a horizontal plane 1 inch (0.0254 m) above the entrance to the tube sheet. The predicted boundary line is typically within one tube of the measured boundary and the general location and shape of the tube boundary are consistent. A review of the complete set of experimental results demonstrates a variation in the tube flow split ratio larger than the difference observed here. These predicted results are considered good in light of these experimental variations.

The experimental results appear to be biased towards reporting too many hot tubes. This bias, if corrected, further increases the difference between the prediction and the experiments. The flow in a tube, hot or cold, is determined by a temperature measurement made 1 inch* (0.0254

* or 5 inch for some tubes

m) above the inlet plenum inside the tube. Temperatures close to the secondary side temperature indicate the tube carries cold return flow. Temperatures above the secondary side temperature are assumed to indicate hot (upward) flow. Approximately 25% of the tubes are instrumented. Some type of judgment is used to assign the tubes with no thermocouple to either a hot or cold flow status. The unmeasured tubes that are positioned directly between a hot and cold tube are assumed to carry hot flow. This biases the result towards a higher number of hot tubes. If one assumes that tubes between a hot and cold tube carry cold flow, the number of hot tubes for test SG-S3 is only 49. This represents a reduction of 26 tubes or 12% of the total tubes in the bundle. It is suggested that the midpoint, 62 hot tubes, of these values may represent the total number of hot tubes for this test. Assuming 62 hot tubes increases overprediction by the CFD model to 9% of the tubes in the bundle. The CFD predictions determine hot and cold flow tubes based upon the velocity profiles 1 m (39.4 inches) above the inlet plenum. The results are not influenced by interpretation since each tube is considered.

T_h, Hot Leg. The hot leg hot-flow temperature is predicted to be 4.3 ^oC below the experimentally observed value. The predicted value can be controlled by the inlet boundary conditions. It is not adjusted to match the experimental value because of differences in the approaches used to obtain this value. The experimental hot leg hot-flow temperature is obtained from a single thermocouple reading located on the center of the upper quarter flow area of the hot leg near the steam generator end of the pipe (x = -0.292 m, -11.5 in.). Based on the CFD predictions, this point is not at a temperature equal to the mass averaged hot leg hot-flow temperature. The predicted hot leg hot-flow temperature is obtained as a mass averaged integral of the forward flow in the hot leg on a vertical plane near the mid-point of the pipe (x = -0.56 m, -22 in.).

Figure 5 illustrates the temperatures in the hot leg used to obtain the value for T_h. The continuous curve represents the CFD prediction on the centerline of the pipe between the lower and upper wall. The predictions indicate that the return flow is at a relatively uniform temperature of approximately 353.2 K on the bottom half of the pipe. The upper portion of the pipe contains the hot flow. The vertical line at a temperature of 428.1 K represents the mass averaged temperature of this forward flow. The diamond (single point) on the plot indicates the measured result (432.5 K). The predicted temperature at the location of the thermocouple is approximately 442 K. This indicates a predicted temperature higher than the measurement.

The limited available data in the hot leg do not allow for refinement of the hot leg hot-flow prediction. The predicted value is considered acceptable in light of the potential uncertainty in the measured value. The measurement uncertainty is affected by the large temperature gradient expected in the region of the thermocouple. A vertical temperature gradient of 4 to 5 ^oC per millimeter (206 ^oF/in.) is predicted at this location. In addition, the single thermocouple measurement is unlikely to be equal to the mass averaged temperature. Detailed velocity and temperature profiles, unavailable from the tests, are needed to assess the measurement.

T_c, Hot Leg. The average temperature of the cold return flow in the hot leg is predicted to be about 6.7 K lower than the measured value. Measured values are obtained from the average value of two thermocouples positioned in the lower half of the hot leg near the steam generator end. The return temperature is observed and predicted to be very uniform. An average vertical temperature gradient of approximately 0.1 ^oC per millimeter is predicted in this region. The predicted hot leg cold-flow temperature is obtained as a mass averaged integral of the return flow in the hot leg on a vertical plane near the midpoint of the pipe (x = -.56 m, -22 in.).

m, Hot Leg. Mass flow in the hot leg is predicted to be 2.3% below the reported value. This value can be adjusted with the hot leg inlet boundary conditions. The value is considered in good agreement and needs no adjustment in light of the suspected experimental uncertainties. The computed mass flow is obtained from an integral of the hot flow near the center of the hot leg (x = -.56 m, -22 in.). The experimental mass flow rate is estimated from the hot leg temperature measurements and the tube bundle energy loss. Tube bundle heat transfer is obtained from measurements of the secondary side coolant mass flow and its associated temperature rise. A steady state 1st law of thermodynamics analysis is used to obtain the tube bundle energy loss. An additional 1st law analysis is used to obtain the hot leg mass flow from the tube bundle heat loss and the measured values of T_h and T_c. This indirect means of obtaining the hot leg mass flow is expected to result in a measurement uncertainty significantly above the 2.3% difference in the predicted value. The uncertainty is not estimated in the data report.

T_{ht} , T_{ct} Tubes. The temperature of the hot flow entering the tubes, T_{ht}, is predicted to be within 1 degree of the measured value. Tube entrance temperatures are a primary result of this analysis. The hot flow, after significant mixing in the inlet plenum, is predicted to have essentially the same temperature as in the experiment as it enters the tube bundle. This result is very encouraging for the prospects of predicting inlet plenum mixing with CFD. The cold-tube return flow temperature, T_{ct}, is essentially equal to the secondary side temperature. This value is established as a boundary condition to match the data exactly.

Tube temperatures in the experiments come from thermocouples located within the tubes 1 inch (0.0254 m) or 5 inches (0.127 m) above the tube entrance. Approximately 25% of the tubes are instrumented. The downflow measurements are essentially equal to the secondary side temperature. This fact makes the up and down flow tubes easy to distinguish. All of the hot thermocouples are identified and a simple average is used to determine the experimental hot-flow temperature entering the tube bundle (T_{ht}). FLUENT predictions of the temperature entering the tube bundle are obtained from a mass weighted integral over the upward flow region at an elevation 1 inch above the tube sheet entrance.

m_t Tubes. Mass flow through the tube bundle is predicted to be within 1% of the experimental value. The agreement lends credibility to the modeling approach used for the tube bundle. The predicted mass flow is obtained from an integral of the mass flux over the region of upward flow in the bundle. This integral is completed 1 m (39.4 in.) above the tube sheet. Experimentally, the tube bundle mass flow is determined from a steady state 1st law of thermodynamics analysis. The tube bundle heat loss and the tube entrance and exit temperatures are used to find the mass flow rate.

m_t/m (recirculation ratio). The ratio of the tube bundle mass flow to the hot leg mass flow defines the recirculation ratio. The predicted ratio is about 2.5% above the experimentally reported value. The prediction is considered to be within the experimental uncertainty.

f (mixing fraction). The mixing fraction, f, is defined as the fraction of hot leg (hot) flow that mixes with the cold return flow in the inlet plenum. The formulation for f is given in an associated report[6] (Ebeling-Koning et al., 1990) along with a diagram of flow patterns used to define f. The predicted mixing fraction is 4.7% below the reported value. The formulation given in Reference 6 is used with the CFD predictions to determine the mixing fraction even though the assumptions made to define f may not be ideal. Although the result is very sensitive to small changes in the tube bundle hot flow temperature, the prediction is very consistent with the data.

6.2 Hot Leg Prediction

The hot leg flow consists of an accelerating hot flow stream traveling from the vessel to the steam generator along the top one-half to one-third of the hot leg flow area. Cooler gas returns from the steam generator to the vessel through the lower portion of the hot leg. The flow remains very stratified in the hot leg region. Figure 5 shows the vertical temperature profile at a location near the center of the hot leg. The hot flow occupies the upper 40% of the hot leg (based on height). A large vertical temperature gradient is predicted in the lower portion of the hot flow. The cold return flow temperatures are much more uniform, as shown on the lower portion of the curve. These predictions agree qualitatively with the experimental observations and limited measurements in the hot leg as noted in Reference 2 (p. D-16).

Figure 6 illustrates temperature contours on the hot leg symmetry plane. The uniform cold return flow region is clearly seen on the bottom of the pipe. Vertical profiles of the velocity on the symmetry plane are inset on the figure at two locations (x = -.56 m and x = -.292 m). These profiles illustrate the acceleration of the hot flow as it approaches the steam generator. As the flow accelerates, the hot flow area is reduced. The flow is predicted to continue accelerating into the nozzle region with a peak velocity reached just beyond the nozzle exit (in the inlet plenum). The flow retains a high degree of stratification throughout the hot leg. Temperature contours on a hot leg cross section at x = -0.56 m (-22 in.) illustrate the high degree of thermal stratification.

6.3 Nozzle Region Predictions

The nozzle region plays a significant role in the overall mixing behavior of the system. This is a region of complex flow topology and high thermal and velocity gradients. Significant mixing begins to occur in the nozzle region. This region is at an intersection between the hot and cold flow streams. The hot stream is exiting the hot leg and entering the inlet plenum. The cooler return flow is trying to enter the hot leg and flow towards the vessel. Path lines on the symmetry plane are shown in Figure 7. The hot flow vectors accelerate through the nozzle and flow directly to the tube sheet. Cold return flow intersects the hot plume right at the nozzle exit. This intersection of two streams is indicated on Figure 7. The return flow appears to form a stagnation point on the hot plume with part of the flow becoming entrained into the rising plume and part of the flow entering the hot leg. Inlet plenum flows, described in the next section, further clarify this behavior.

This complex flow behavior significantly increases the level of turbulence in the flow. Figure 8 shows the contours of turbulence intensity on the symmetry plane in the nozzle and inlet plenum region. Turbulence intensity reaches a local maximum at the intersection of the nozzle and the inlet plenum. This location corresponds to the region where the two streams intersect highlighted in Figure 7. The significant result of this complex flow is the resultant mixing of the hot plume as evidenced by the reduction in plume temperature. Figure 9 shows normalized temperature contours in the nozzle and inlet plenum region. The hottest temperatures remain in the range between 1.2 and 1.3 for the entire hot leg length. Significant temperature reduction begins to occur at the junction between the nozzle and the inlet plenum. The isotherms are very close together in this region. The normalized temperature is reduced to 0.55 just below the tube sheet entrance. These data are consistent with experimental observations that indicate a significant temperature reduction close to the nozzle region. It is noted that the normalized

temperature for the mass averaged hot leg hot flow is 1.0. Peak hot leg temperatures are higher than this mass averaged value.

6.4 Inlet Plenum Flows

The steam generator inlet plenum is the region associated with the mixing phenomena of interest in this study. As noted earlier, this mixing begins to occur significantly in the nozzle region. The hot plume leaving the nozzle rises quickly through the inlet plenum and impacts the face of the tube sheet. Part of this flow enters the tube bundle and flows to the outlet plenum of the steam generator. Another portion of this flow stagnates and turns radially outward from the point of intersection. This behavior is similar to a stagnation flow on a porous surface. The flow that remains in the inlet plenum flows radially towards the inlet plenum walls. The flow on the symmetry plane is shown in the path lines of Figure 7. There are significant mixing flows in planes perpendicular to the symmetry plane. Figure 10 shows flow vectors on three vertical planes normal to the symmetry plane. As the hot plume intersects the tube sheet, flow is directed towards the walls of the inlet plenum and then down and around the spherical walls. Flows from both sides intersect at the bottom of the inlet plenum and are directed upward again. This behavior explains the upward flow paths evident over much of the inlet plenum symmetry plane in Figure 7. Two large recirculation regions are formed in the inlet plenum as shown in Figure 10.

The plume spreading is minimal until the plume intersects the tube sheet and spreads out in all directions. Figure 11 shows temperature contours on three horizontal (y) planes. The y coordinate value of each plane is noted on the figure along with the relative locations of the plane within the inlet plenum. The lower plane (y = -5.5 in.) shows the region of the plume just above the elevation of the nozzle. The plume is very small and the remainder of the inlet plenum is at a significantly lower temperature. In the next plane shown, y = -2 in., the plume temperature is reduced but the plume is still occupying only a small region of the inlet plenum. The upper plane is located just 0.25 inches below the tube sheet. At this elevation, the plume has impacted the tube sheet and is spreading in all directions. The region of impact is identified by the hottest temperature zone at the center. The extent of the spreading can be clearly seen at this level. The spreading layer is pushed downward by the returning flow from the outlet plenum and the hot layer drops below the 0.25 inch level shown in the top plane.

Similar behavior is illustrated in Figure 12 in vertical planes parallel to the symmetry plane. Three planes are shown with z coordinates of 0, -2, and –5.5 inches. Temperature contours on the symmetry plane, z = 0, show the path of the plume and the spreading of the hot flow as it encounters the tube sheet. On a plane just 2 inches away, the plume is not evident. The hot layer near the tube sheet is the only evidence of the hot plume. The colder return flow from the tubes enters the inlet plenum and is entrained by the inlet plenum flows. Some of this return flow is evident by the cooler temperatures at the upper most portion of the plane at z = -5.5 inches.

6.5 Tube Bundle Flows

Part of the tube bundle carries hot flow from the inlet to the outlet plenum. The remaining tubes carry the cooler return flow back to the inlet plenum. The hot tubes loose their heat to the secondary side coolant at a rate that reduces the hottest tubes to temperatures near the secondary side temperature by the time the flow reaches the top of the tube bundle. Beyond this

point, the forward flow and the return flow tubes are at a temperature equal to the secondary side coolant. This is consistent with the test setup but does not represent prototypical behavior.

Figure 4 (adapted from Reference 6) shows the boundary between the hot and cold tubes. The CFD results overpredict the number of hot tubes by more than 3%. Generally speaking, the predicted region of hot tubes is consistent with the data and the wider range of experimental observations. Figure 13 shows the temperature contours on a horizontal plane 1 inch above the tube sheet entrance. The hot tube region is clearly visible on the figure. The cold tubes, with black contours, are all at a uniform temperature equal to the secondary side coolant temperature. Some cold tubes on the boundary between the hot and cold tubes show a small amount of hot gas in a portion of the tube region. These tubes had a small return flow velocity and hot gas penetrated into the tubes a small distance as indicated in the figure. This is probably the result of the tube modeling approach that utilized tubes of increased cross section† to simplify the mesh requirements.

A peak temperature is found at the center of the hot tube region in Figure 13 and the temperature drops off from that point. To quantify the temperature variations in the hot flow tubes, a histogram is created to show the relative number of tubes within a series of temperature ranges. Figure 14 gives the percentage of tubes in the tube sheet that fall into specific normalized temperature ranges. Temperatures are normalized by the total temperature difference between the hot leg hot-flow temperature (T_h) and cold tube return flow temperature (T_c). The normalized scale ranges from 0 to 1 and is broken down into 20 ranges (5% each). The center point of each region is indicated on the horizontal axis. Only hot flow tubes are shown on the histogram and the tube percentages are based upon the total number of tubes in the bundle. The summation of the value for each range equals 38%. The data indicate that the normalized temperature entering the tube sheet fall within the normalized temperature range of 0.15 – 0.55. The largest group of tubes, just over 10% of the total, falls in a normalized temperature band centered on 0.375 (range from .35 - .40). Only 2.3% of the tubes fall into the highest range between 0.5 and 0.55. These maximum values demonstrate the effectiveness of the inlet plenum mixing for reducing the temperature of the hot gas reaching the tube bundle.

Figure 15 shows temperature profiles for the entire symmetry plane of the model. The hot gas in the tube bundle approaches the secondary side temperature prior to reaching the top of the tube bundle. This is consistent with the experimental observations from the steady state tests. These temperature observations from the test program were used to establish the rate of heat transfer from the tube bundle model. Appendix A should be reviewed for details of the approach used to model the tubes.

6.6 Sensitivity Study Results

Sensitivity studies are completed to quantify the effect of variations in the input parameters to look for values where uncertainty can significantly affect the solution. Table 5 lists the conditions used for the sensitivity studies. Solution sensitivities are considered for variations of the hot leg inlet temperature, hot leg inlet velocity, turbulence model, tubesheet pressure drop, viscous tube losses, and the tube external heat transfer coefficient. Specific results from the sensitivity studies are listed in Table 6. Each sensitivity study prediction results in the same general flow behavior as the base case outlined above. No fundamental changes in the flow structure are

† See Appendix A.

predicted. Specific values for flow variables and mixing parameters are affected by the variations in the input parameters and will be quantified. Table 6 lists the values predicted for specific parameters along with an indication of the change in the value in relation to the base case result. Each of the sensitivity studies is discussed in more detail below.

6.6.1 Inlet Temperature Sensitivity

The inlet temperature sensitivity is completed with the temperature at the hot leg inlet set to 432.45 K (318.7 ^{o}F). All other modeling options and input parameters are equivalent to the base case described earlier. This inlet temperature is 15 K (28 ^{o}F) lower than the base case boundary condition. Generally speaking, this analysis does not reveal a significant sensitivity. The flow patterns and most of the predicted parameters in Table 6 are very close to the base case prediction. The variations predicted are consistent with the change made to the boundary conditions.

The largest change, other than the obvious hot leg temperature reduction, is the 13 % reduction in the tube bundle heat loss. This reduction results from the combination of a reduced tube bundle mass flow and a reduced tube bundle entrance temperature. Tube bundle entrance temperature, T_{ht}, is predicted to be 2.9 K (5.2 ^{o}F) below the base case result. The 2.9 K drop in the entrance temperature reduces the total temperature drop for the tube flows by 8.2% compared to the base case. Tube bundle heat loss is proportional to this temperature drop and the tube bundle mass flow. Tube bundle mass flow is reduced by 5.9%. A drop in the tube bundle mass flow is expected due to the lower temperatures and resulting lower buoyancy forces.

The 15K (28 ^{o}F) temperature drop at the boundary results in a 10.3 K (18.5 ^{o}F) drop in the mass averaged hot leg temperature. There is apparently less hot leg mixing and entrainment in the lower temperature case. At the tube sheet entrance, the temperature reduction is only 2.9 K (5.2 ^{o}F), as noted earlier. This does not appear to be a significant reduction given the 15 K decrease at the boundary. The results look more consistent in dimensionless form. Using reference temperatures specific to each case, the dimensionless tube entrance temperature for the base case is 0.391 and for this sensitivity study the result is 0.405. These values are within 3.6% of each other.

6.6.2 Hot Leg Inlet Mass Flow (Inlet Velocity) Sensitivity

The hot leg inlet mass flow is increased by 20% for this sensitivity. The increase is achieved by increasing the inlet velocity by 20% without changing the inlet temperature. The general behavior of the system is similar to that described earlier for the base case. In general, the higher velocities in the hot leg resulted in increased mass flows throughout the system.

The hot leg mass flow predicted at the middle of the pipe increases by 11.4%. The higher velocity in the hot leg results in additional flow reversal (entrainment). Some of the increased mass flow reverses in the hot leg and flows back towards the vessel prior to reaching the steam generator. Some limited additional analysis, not reported here, indicates that further increases in the inlet velocity result in ever-increasing amounts of flow reversal in the hot leg with little or no increase in the net mass flow to the inlet plenum. These higher velocity inlet conditions are reaching the countercurrent flow limitations for this model.

The increase in the hot leg velocity does not affect the path of the rising hot plume. Buoyancy forces still dominate the plume behavior. The plume is predicted to rise through the inlet plenum on essentially the same trajectory as in the base case. The number of hot flow tubes in the bundle and the pattern of hot tubes is unchanged. The increased hot leg mass flow increases the mass averaged temperature in the hot leg by over 5 K (9 ^{o}F). This increase in temperature increases the buoyancy forces in the inlet plenum and accounts for the 7.7% increase in the tube bundle mass flow. The increase in the tube bundle mass flow is not quite as large as the increase in the hot leg flow and the resulting recirculation ratio is 3.4% below the base case prediction. The mass averaged temperature entering the tubes is 3.2 K (5.8 ^{o}F) higher than the base case. This value results in an averaged dimensionless temperature entering the tubes of 0.404. This value is consistent with the base case and inlet temperature sensitivity study discussed earlier.

6.6.3 Turbulence Model Sensitivity

The second order Reynolds stress turbulence model is selected for this analysis for the reasons stated earlier in this report. This decision is not based upon a detailed analysis of the flowfield since these data are not available from the experiment. To quantify the effect that the choice of the turbulence model can have, the base case is modified to use a first order k-epsilon type turbulence model. The RNG k-epsilon turbulence model is used along with full buoyancy effects and nonequilibrium wall functions to remain consistent with the base case.

Qualitatively, the results and flow patterns are similar. The predicted parameters are generally within 5% of the base case. One notable exception is the mixing fraction that is over 12% higher than the base case. K-epsilon type turbulence models have a tendency to overmix under many conditions and it is suspected that this characteristic is evident in these results. This particular model also predicted significantly more lower tube recirculation. In a small portion of the tubes, hot gas enters the tubes and rises for a short time before some of it is cooled and returns directly to the inlet plenum. It is assumed that this phenomenon occurs due to the large tube cross sections associated with the tube bundle modeling approach. This phenomenon is not expected to occur in the experiments due to the small tube cross sections associated with the facility. This type of recirculation can help increase the tube bundle heat loss. A detailed analysis of the effects of the turbulence modeling approach is beyond the scope of this report.

6.6.4 Tube Sheet Entrance Pressure Loss Sensitivity

The simplified tube model used for this analysis assumes the tube sheet entrance pressure drop is proportional to the local flow velocity squared. The tube bundle model and this relationship are described in Appendix A. For this sensitivity study, the tube entrance pressure drop coefficient is increased by 25%. For a given flow velocity, this change creates a tube bundle entrance pressure drop 25% higher than the base case. This results in no significant variation in the predicted results. Key mixing parameters are within 2% of the base case results. This increase in the pressure drop decreased the tube bundle flows by only 2.2%. Tube bundle entrance pressure drop accounts for only a fraction of the total pressure drop for flow through the tubes. Most of the total pressure drop comes from the viscous (shear) losses to the tube wall. This sensitivity study demonstrates that a small amount of uncertainty in the tube entrance pressure loss coefficient does not significantly impact the overall solution.

6.6.5 Tube Flow Viscous Loss Sensitivity

The tube bundle modeling approach defined in Appendix A relies on coefficients to model the viscous pressure drop for flow in individual tubes. This sensitivity study increases these coefficients by 25% over the base case. The most significant change is a 10.7% reduction in the tube bundle mass flow and a related 9.2% drop in the recirculation ratio. This result is not surprising since the resistance to flow in the tube bundle is predominantly made up from the tube flow viscous losses. Surprisingly, the number of hot tubes and other parameters are not significantly affected by this change in the tube bundle flow resistance. Fortunately, tube flow viscous losses for single-phase flow are predicted with a relatively low level of uncertainty. The results of this sensitivity study provide confidence that small uncertainties in the tube flow viscous loss determination do not adversely affect the overall results.

6.6.6 Tube Heat Transfer Coefficient Sensitivity

The heat transfer coefficient on the outside of the tubes (secondary side boundary condition) is changed for a pair of sensitivity studies related to this important parameter. The results indicate that this boundary condition plays a significant role in the determination of the mixing parameters of interest. This is the only sensitivity study completed that affects the predicted number of hot tubes. In addition, the largest changes in the recirculation ratio and the mixing fraction result from these changes. The heat transfer coefficient on the tube secondary side is predicted to be a key parameter governing the flow and mixing behavior of this type of scenario.

Heat transfer coefficients in complex geometries are difficult to determine without detailed experiments. Natural circulation flows on the secondary side of the tubes are assumed to be complex in nature. There is a potential for large uncertainties in the secondary side heat transfer coefficients. The results of this sensitivity study indicate that an effort should be made to reduce the uncertainty in the secondary side heat transfer coefficients used for this type of modeling approach due to the significant impact these conditions have on the predicted mixing parameters.
The base case utilized a heat transfer coefficient of 250 W/m^2-K on the outer surface of each tube. This value cannot be compared directly to the experimental heat transfer coefficient due to the nature of the tube bundle model. This value is established, along with other tube bundle thermal properties, to provide an equivalent rate of heat loss from the tubes. Sensitivity studies are completed with the heat transfer coefficient set to 5000 and 100 W/m^2-K. The 5000 W/m^2-K case is chosen to be large enough to effectively set the tube outer wall temperature to the secondary side temperature. The value of 100 W/m^2-K reduces the heat transfer coefficient by a factor of 2.5.

The first interesting result is the effect these changes have on the net tube bundle heat loss. The heat loss decreases when the heat transfer coefficient is increased. Tube bundle heat loss increases when the heat transfer coefficient is decreased. The tube bundle flows help explain the differences in the tube bundle heat loss. The increased heat transfer coefficient results in the tube flows reaching the secondary side temperature over a shorter length of tube. This results in a shorter column of hot gas that provides the buoyancy driving force. A small tube bundle mass flow is the result. Likewise, the decreased heat transfer coefficient results in a larger vertical column of hot gas that produces a larger buoyancy driving force. The tube bundle mass flow is increased in this case. For a given temperature change, the tube bundle heat loss is proportional to the tube bundle mass flow rate. Tube bundle mass flow rates changed by an

average of 16.8% for these sensitivity studies. The resulting average change in the recirculation ratio is 14.8%.

The number of hot tubes changed as a result of the changes in the heat transfer rate. More tubes carried hot flow in the case where the heat transfer coefficient is decreased. It is suggested that the reduced heat transfer rate, and the resulting reduction in the tube bundle mass flow, cause the rising hot plume in the inlet plenum to spread further when it intersects the tube sheet. This increased spreading is suspected to be the cause of the increase in the number of hot tubes. The flow pattern of the plume intersecting the tube sheet is a combination of a stagnation flow and a penetrating flow. If the tube bundle flows are retarded due to a smaller buoyancy force, the amount of penetrating flow is reduced and the stagnation flow pattern (spreading) is enhanced. The mixing fraction relates to the portion of the flow from the hot leg that mixes into the inlet plenum without directly penetrating into the tubes. This increase in the mixing fraction for the case with increased heat transfer is consistent with the analogy of the stagnation and penetrating flows. Increases in the buoyancy driving force make it easier for the rising hot plume to penetrate into the tube bundle and therefore result in decreases in both the number of hot tubes and the mixing fraction.

7 SUMMARY

The best estimate prediction at 1/7th scale demonstrates the applicability of the modeling approach used along with the FLUENT CFD code to predict severe accident natural circulation flow and mixing parameters in the steam generator inlet plenum. Best estimate predictions are qualitatively consistent with the experimental observations. The overall flow pattern and behavior are correctly predicted. Quantitative comparisons demonstrate the capability to predict key mixing parameters for this type of scenario. A series of sensitivity studies demonstrates that the solution is not adversely affected by the uncertainty in key modeling parameters and boundary conditions. The most significant modeling input is predicted to be the secondary side heat transfer coefficient. This input parameter has a significant impact on the three key mixing parameters (# hot tubes, mixing fraction, and recirculation ratio). It is suggested that the secondary side heat transfer is the key boundary condition that must be well defined in order to carry out this type of modeling. The qualitative and quantitative agreement between the data and the predictions confirms the applicability of the FLUENT code to predict the severe accident natural circulation flow and mixing behavior in the hot leg and steam generator. There are no foreseen limitations for applying this technique to similar scenarios beyond the range of the existing experimental data.

8 REFERENCES

1. Memorandum on the steam generator action plan from Ashok Thadani and Samuel Collins to William Travers, dated May 11, 2000.

2. P. D. Bayless et al., “Severe Accident Natural Circulation Studies at the INEL,” NUREG/CR-6285, INEL-94/0016, February 1995.

3. SGTR Severe Accident Working Group, “Risk Assessment of Severe Accident-Induced Steam Generator Tube Rupture,” NUREG-1570, March 1998.

4. Westinghouse Electric Corporation, “Natural Circulation Experiments for PWR High-Pressure Accidents,” Research Project 2177-05, Final Report, August 1993.

5. J. D. Anderson, *Computational Fluid Dynamics: The Basics with Applications*, McGraw-Hill Series in Mechanical Engineering, McGraw Hill, 1995.

6. D. B. Ebeling-Koning et al., “Steam Generator Inlet Plenum Mixing Model For Severe Accident Natural Circulation Conditions,” 1990 ASME Winter Meeting, Dallas, Texas.

APPENDIX A

STEAM GENERATOR TUBE MODEL
POROUS MEDIA APPROACH

A.1 BACKGROUND

The computational fluid dynamics (CFD) analysis documented in this report uses a porous media approach to model each steam generator tube. This approach is used to reduce the amount of computer resources required to model the tubes. The overriding goal of the CFD model is to determine inlet plenum mixing phenomena. The tube bundle is a boundary condition for the inlet plenum. The tube bundle model must provide an appropriate tube bundle mass flow and pressure boundary condition such that the inlet plenum flows are well represented. Tube bundle flows result from a balance between the buoyancy driving forces and the inertial and viscous pressure loss terms. The modeling approach used here seeks to provide a model to reproduce each of these characteristics with a minimal number of nodes.

Modeling the tubes directly is estimated to require 8 million cells. This makes a detailed study impractical. To simplify the mesh, each tube is modeled as a rectangular channel and is defined as a porous medium. The porous media formulation in the FLUENT CFD code provides a means of modeling the pressure drop at the tube sheet inlet and the shear flow viscous losses along the tube with simple algebraic relations. In addition, porous material properties can be established to provide the desired heat transfer characteristics. Resolution of the tube boundary layers and tube entrance effects is unnecessary. The rectangular cross section is used to further reduce the mesh requirements since many hexagonal elements are needed to accurately define a circular cross section.

Three different models, available within the FLUENT modeling formulation, are relied on to establish the tube bundle model. One model, Equation A-1, applies a volume-based source term to the momentum equation to simulate the pressure loss through a porous region. This model is used to represent the viscous flow losses along the tubes.

$$\frac{d\mathrm{p}}{d\mathrm{x}} = \mathrm{D} \cdot \mu \mathrm{V} + \mathrm{C} \cdot \frac{1}{2} \rho \mathrm{V} \cdot |\mathrm{V}| \qquad \text{A-1}$$

The first term in Equation A-1 represents viscosity-dominated losses and the second term provides a higher order term. In three dimensions, the coefficients C and D are matrices to allow for nonisotropic behavior.

The second model, Equation A-2, utilizes a surface-based source term to create a step change in pressure. This equation is used to model the form losses that occur as flow enters and exits the tubes at the tube sheet.

$$\Delta \mathrm{p} = -\left(\frac{\mu}{\alpha} \mathrm{V} + \mathrm{C}_2 \cdot \frac{1}{2} \rho \mathrm{V}^2 \right) \Delta \mathrm{m} \qquad \text{A-2}$$

A final equation from FLUENT's porous model formulation is used to establish the effective thermal conductivity, k_{eff} (Equation A-3).

$$k_{eff} = \Phi \cdot k_f + (1 - \Phi) k_s \qquad \text{A-3}$$

This equation is used to enhance the heat transfer within the tubes to make up for the increased tube cross section.

A.2 GEOMETRY

The tube bundle of the Westinghouse 1/7th scale facility[2] consists of 216 U-shaped tubes with a 0.007747 m (0.305 in.) inner diameter and a 0.009525 m (0.375 in.) outer diameter. The tubes are anchored into a 0.1143 m (4.5 in.) thick tube sheet that caps off the inlet and outlet plenums. Furthermore, the tubes are arranged into a 0.02064 m (0.8125 in.) triangular pitch array. The average tube length is 2.499 m (98.403 in.) and the overall bundle height is 1.124 m (56.06 in.) from the face of the tube sheet.

In the FLUENT model, rectangular cross section tubes and a porous media approach are used to represent the individual tubes of the Westinghouse facility. Each tube modeled in FLUENT represents the flow path and heat transfer characteristics for a single tube in the 1/7th scale facility. Figure A-1 shows a section of tubes from the Westinghouse 1/7th facility that are meshed directly and a corresponding section of the tubes meshed for use with a porous media approach. The symmetric tube section shown in Fig. A-1a includes one complete tube in the center and four one-quarter-tube sections at the corners. The porous media model of this section in Fig. A-1b represents the same region. In the final CFD model, the porous tubes were smaller and only represented a single tube.

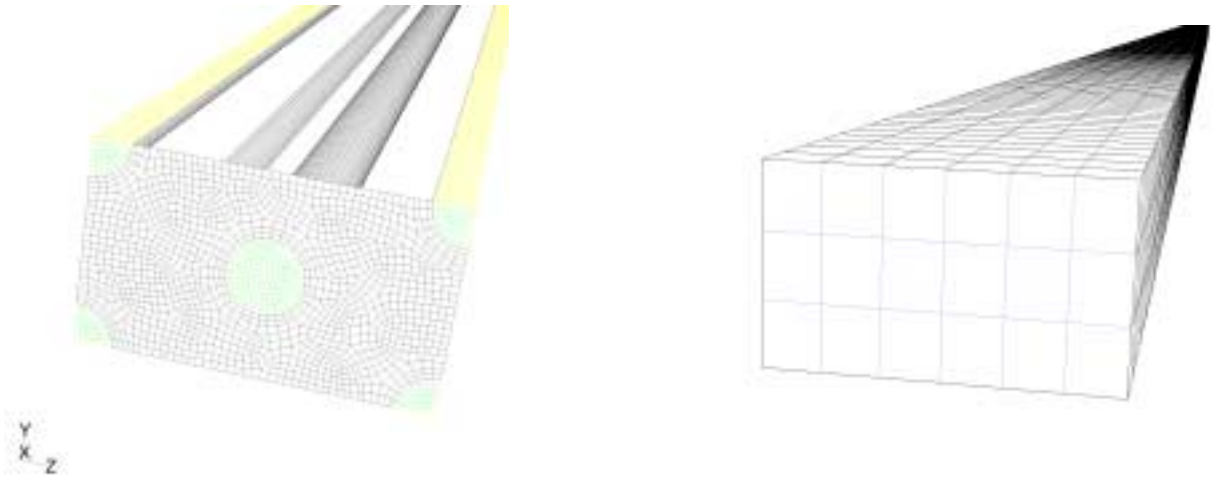

(a) (b)

Figure A-1. (a) Meshed Region of Westinghouse 1/7th Scale Round Tube Model
(b) Mesh used for Equivalent Porous Media Model

A.3 LOSS COEFFICIENT DETERMINATION

The loss coefficients needed in Equations A-1 and A-2 are determined from the detailed model in Fig. A-1a. Predictions for the viscous sheer loss along the tube, dp/dx, and the tube entrance and exit loss, Δp, are determined from this model. Using dp/dx and Δp over a range of velocity and temperature values, the coefficients needed to define the porous model (C, D, and C_2) are found. The pressure drop at the tube sheet is directly proportional to V^2. For this reason, the parameter α is set to 10^{12} to effectively reduce the first term in Equation A-2 to 0. To check the results, dp/dx and Δp are predicted using a porous model (Fig. A-1b) with the porous media coefficients coming from the curve fits.

A pressure drop occurs as fluid enters the tubes and a slight recovery occurs as the fluid exits. Modeling restrictions in FLUENT make it difficult to simulate this phenomenon. The pressure change through the tube sheet is always negative in the porous model. To model the pressure drops, a net pressure drop is determined that includes the entrance and exit effects. The pressure drop at the tube entrance and exit is then defined as half the net pressure drop for a combined loss consistent with the expected behavior.

A.3.1 Viscous Loss Coefficients

The data used to define and validate the viscous loss coefficients are given in Table A-1.

Table A-1. Data for Determination of Viscous Loss Coefficients and Results

V_{in} (m/s)	T_{in} (K)	$\frac{1}{2}\rho V^2$ (kg/m·s^2)	μV (Pa·m)	Fig. A-1a $\left(\frac{dp}{dx}\right)_{ROUND}$ (Pa/m)	Fig. A-1b $\left(\frac{dp}{dx}\right)_{POROUS}$ (Pa/m)
0.03375	375.0	0.0591	6.716E-7	-13.8	**-14.9**
0.0675	375.0	0.2365	1.343E-6	-43.2	**-45.5**
0.1350	375.0	0.9459	2.687E-6	-158.0	**-157.0**
0.03375	315.0	0.0814	5.984E-7	-16.9	**-17.0**
0.0675	315.0	0.3257	1.197E-6	-53.5	**-56.0**
0.1350	315.0	1.303	2.394E-6	-200.0	**-**

For each boundary condition combination (V_{in}, T_{in}), the pressure gradient is predicted in a round tube with a well-defined mesh (Figure A-1a). A multidimensional curve fit of $(dp/dx)_{ROUND}$ versus $\frac{1}{2}\rho V^2$ and μV is used to fit Equation A-1. Coefficients C and D are found to be 137.9 and 9.0920E+6, respectively. Using these values in a porous model, Figure A-1b, the pressure gradients are predicted again and listed in the last column of Table A-1. The results demonstrate that the porous tube model with relatively few cells can accurately produce the viscous pressure drop within the tubes.

A.3.2 Form Loss Coefficient

FLUENT uses the porous jump coefficient, C_2, of Equation A-2 to determine the inertial losses of the porous media model. The input parameters and total pressure loss of the tubes are listed in Table A-2 below.

Table A-2. Values Used To Determine Inertial Loss Coefficient

V_{in} (m/s)	T_{in} (K)	$½\rho V^2$ (kg/m·s^2)	Δp_{ROUND} (Pa)	Δp_{POROUS} (Pa)
0.03375	375.0	0.0591	-5.3	**-4.95**
0.0675	375.0	0.2365	-19.4	**-21.5**
0.1350	375.0	0.9459	-79.0	**-86.0**
0.03375	315.0	0.0814	-7.0	**-7.20**
0.0675	315.0	0.3257	-27.5	**-29.5**
0.1350	315.0	1.303	-108.0	**-**

In Table A-2, the total pressure drop through the tube is listed for both the round and porous media tubes, Δp_{ROUND} and Δp_{POROUS}, respectively. The data labeled Δp_{ROUND} come from the model shown in Fig. A-1a. The model coefficient, C_2, determined from these data is 41.6. This porous coefficient is used to define the inertial loss in the porous media tube model, Fig. A-1b. The results are given as the last column in Table A-2. The porous model is in good agreement with the data.

A.4 THERMAL PROPERTIES

Tube heat transfer characteristics are also considered for the porous media approach. A porous tube with a relatively large cross section is used to represent each tube. The larger cross-sectional area reduces the heat transfer effectiveness. Early attempts to model the tubes with no heat transfer augmentation demonstrated that the heat transfer from the tubes was too low even with an infinite heat transfer coefficient on the secondary side. To boost the heat removal rate, the effective conductivity in the tubes is increased (see Equation A-3).

The fluid phase thermal conductivity, k_f, is defined by the temperature dependant fluid properties of sulfur hexafluoride. The porosity of the medium, ϕ, and the solid medium thermal conductivity, k_s, are inputs to the porous model that are used here to augment the effective conductivity of the tubes. Data from the Westinghouse 1/7th scale facility indicate that tube temperatures essentially reach the secondary side temperature as the flow reaches the top of the tube bundle. Further details are not available. The porosity and solid conductivity are adjusted to establish this experimentally determined condition. The thermal conductivity and porosity of the solid medium in this report are 1.5 W/m^{2}K and 0.75, respectively. One other factor controlling the tube thermal behavior is the tube external heat transfer coefficient. This is not part of the porous model but does play a role. The heat transfer coefficient, h, is set to 250 W/m^2-K for the external surfaces of each of the tubes above the tube sheet.

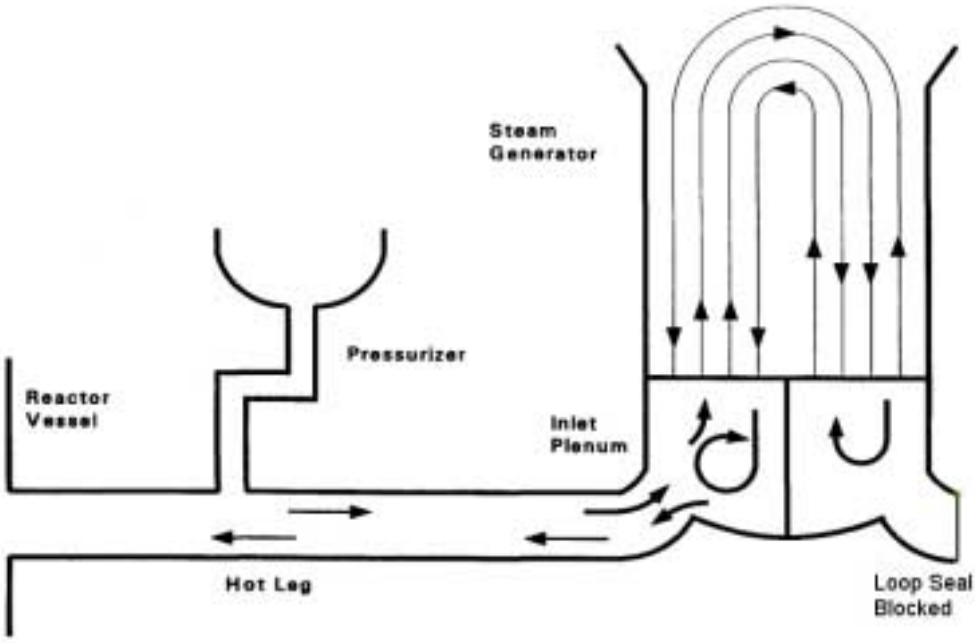

Figure 1. Overview of Natural Circulation Flow Pattern

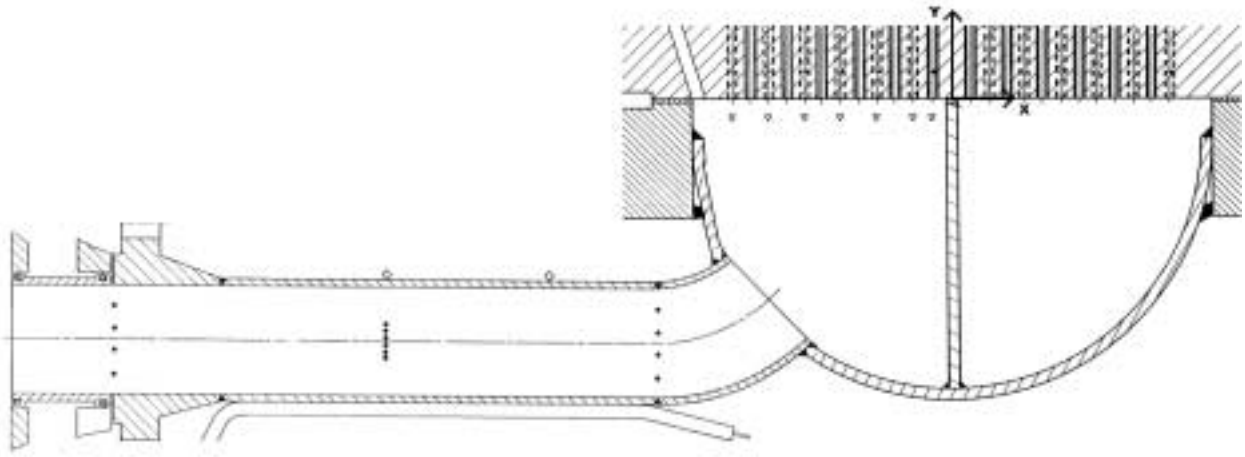

Figure 2. Cross Section of Inlet Plenum, Hot Leg, and Tube Sheet

Figure 3. Computational Mesh

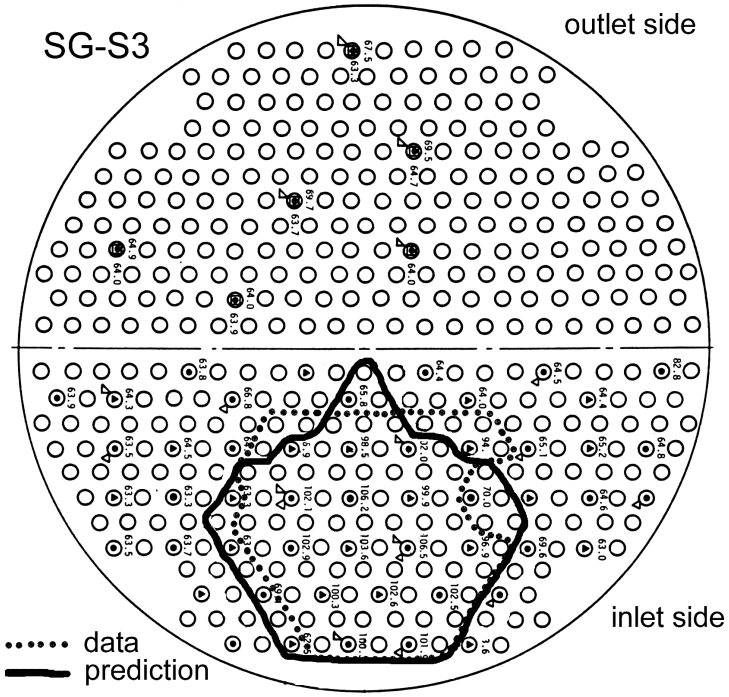

Figure 4. Boundary Between Hot and Cold Tubes

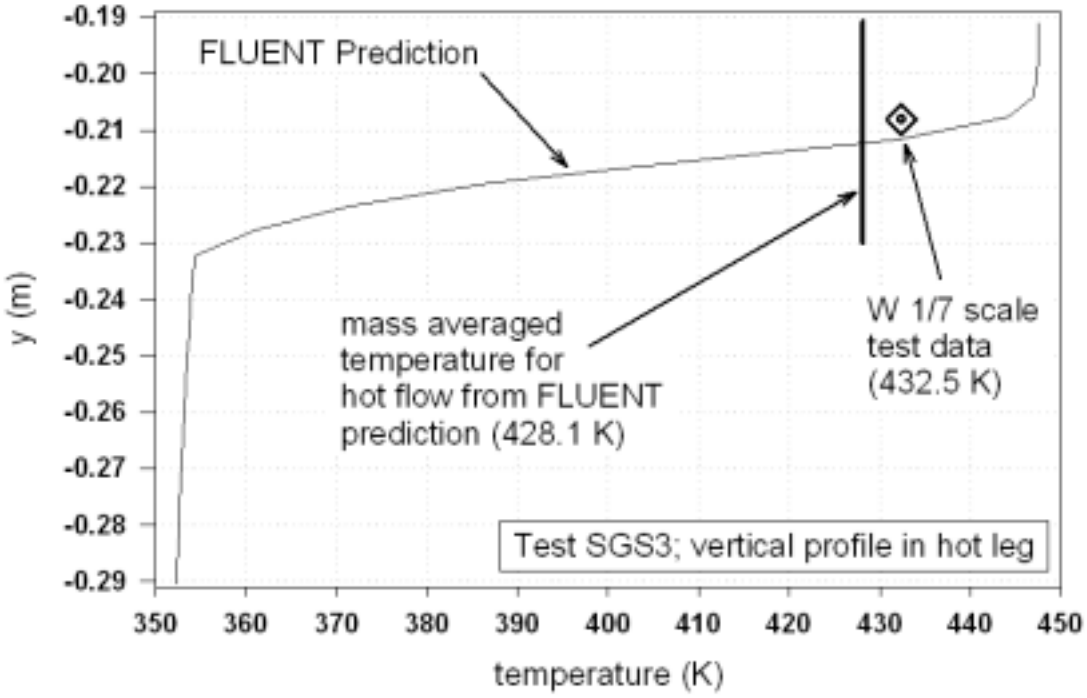

Figure 5. Hot Leg Temperature Prediction and Data (x = -0.566 m)

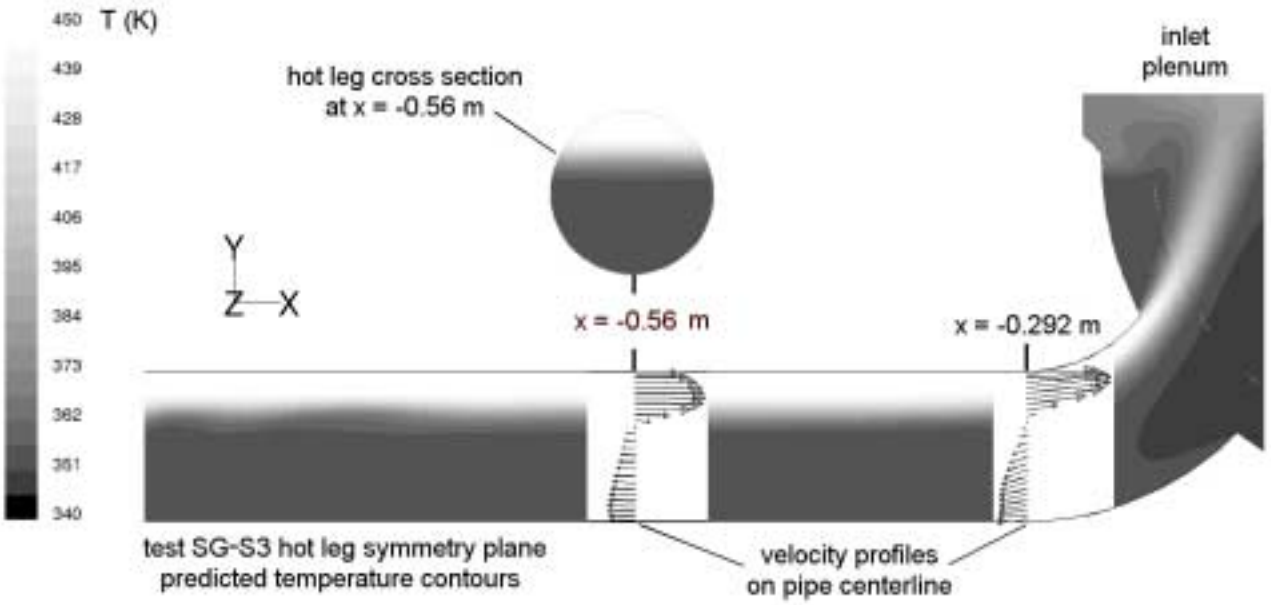

Figure 6. Hot Leg Temperature Contours and Velocity Profiles

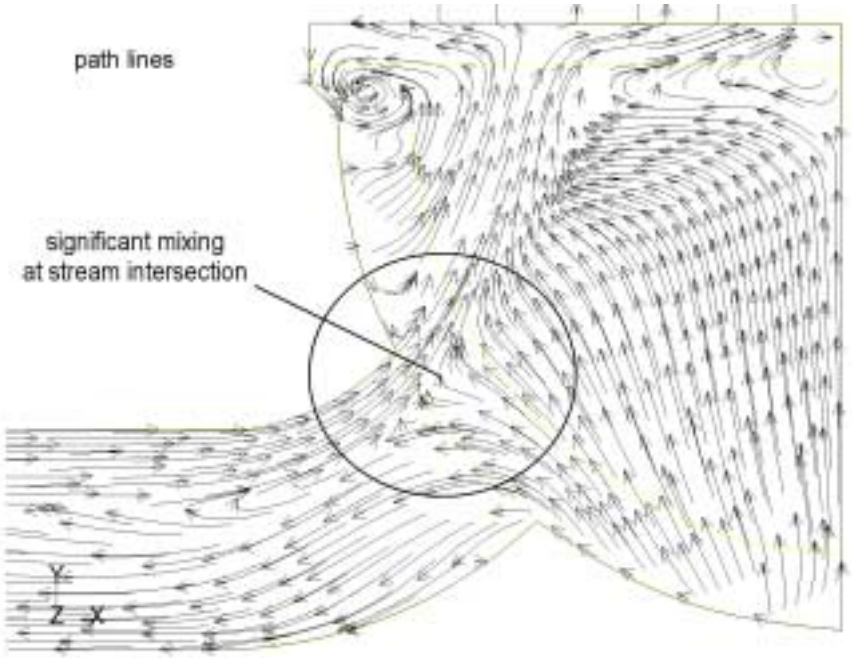

Figure 7. Path Lines on Symmetry Plane of Inlet Plenum

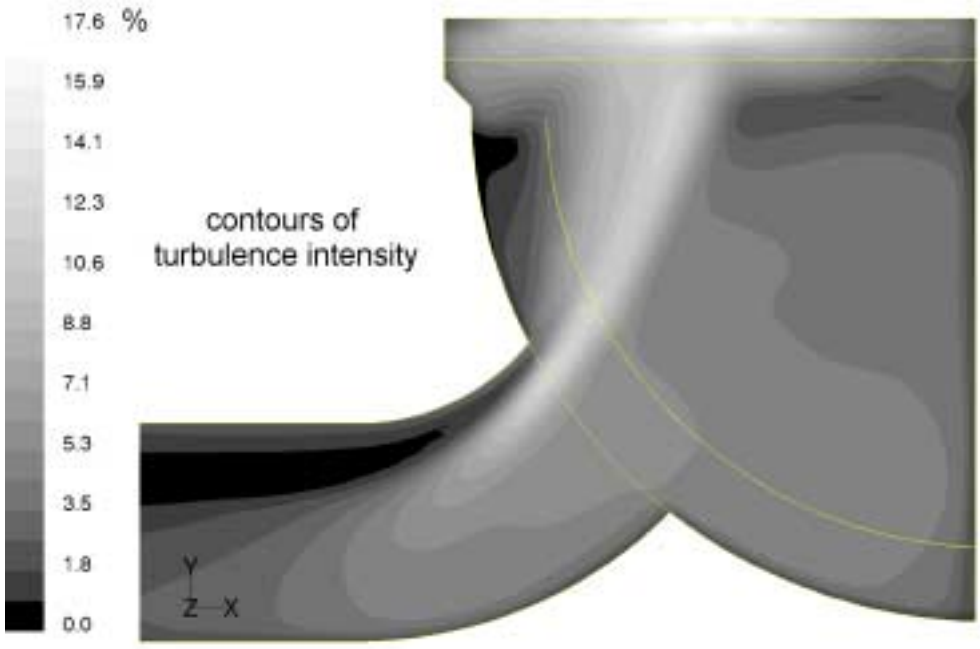

Figure 8. Contours of Turbulence Intensity on Symmetry Plane of Inlet Plenum

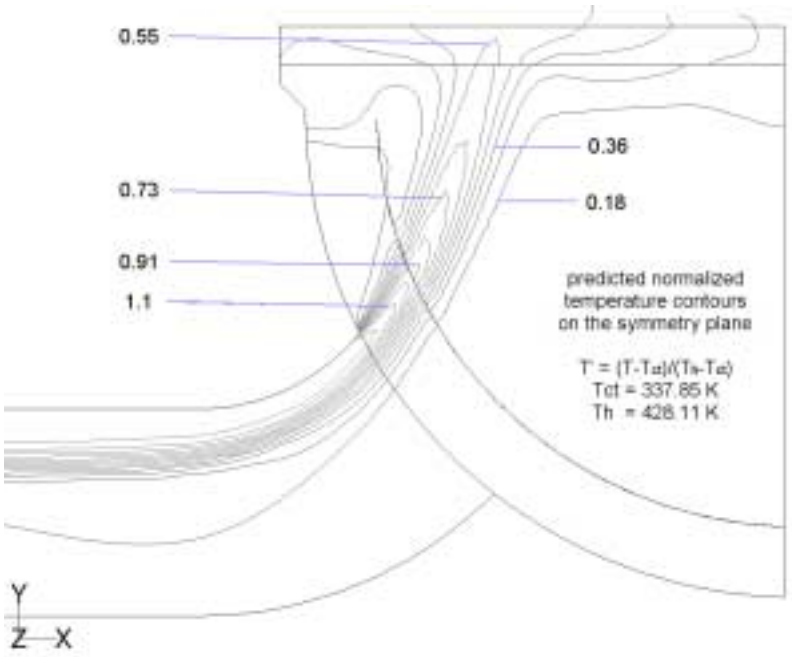

Figure 9. Normalized Temperature Contours on Symmetry Plane of Inlet Plenum

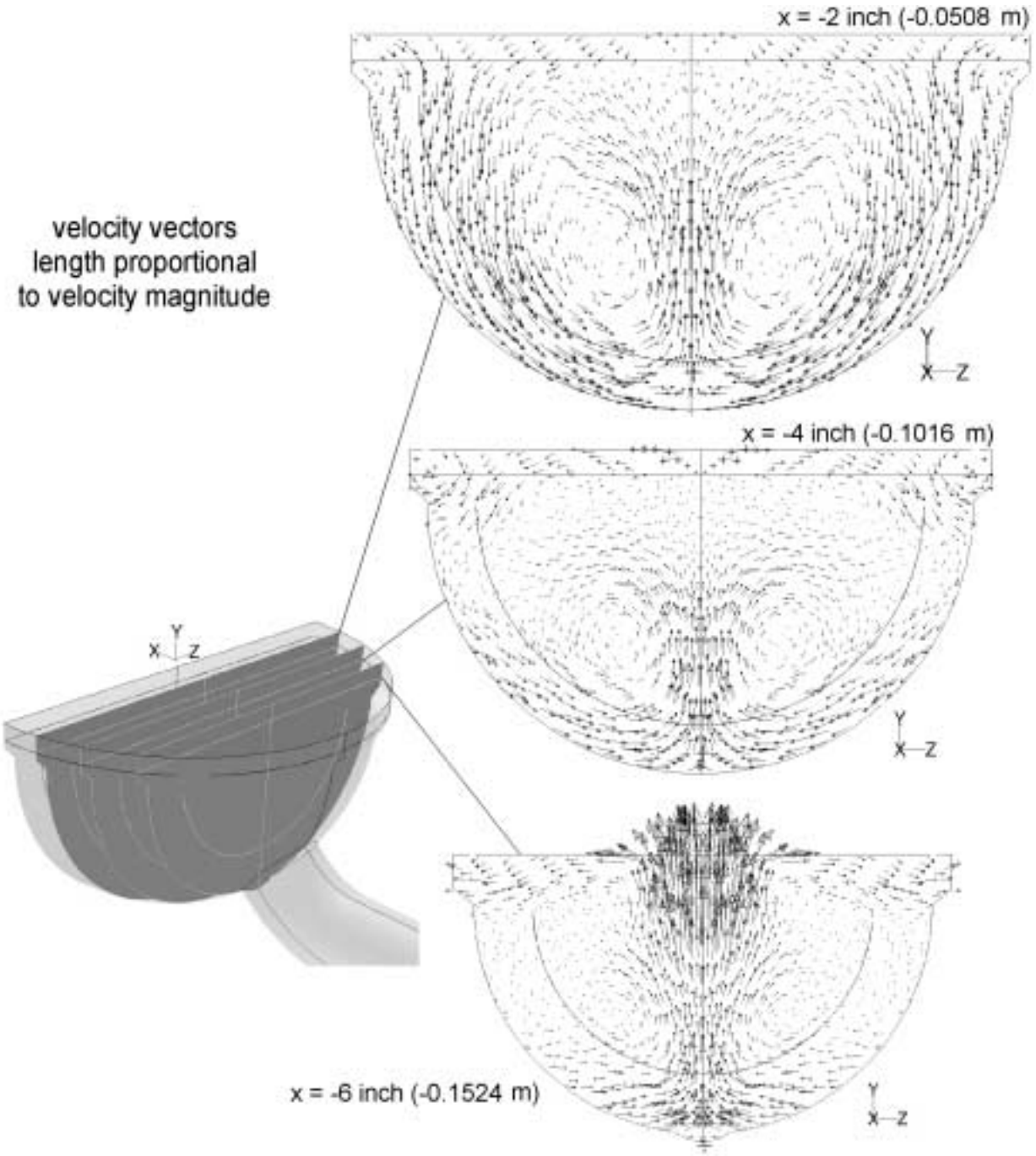

Figure 10. Velocity Vectors on Vertical Planes Normal to Symmetry Plane

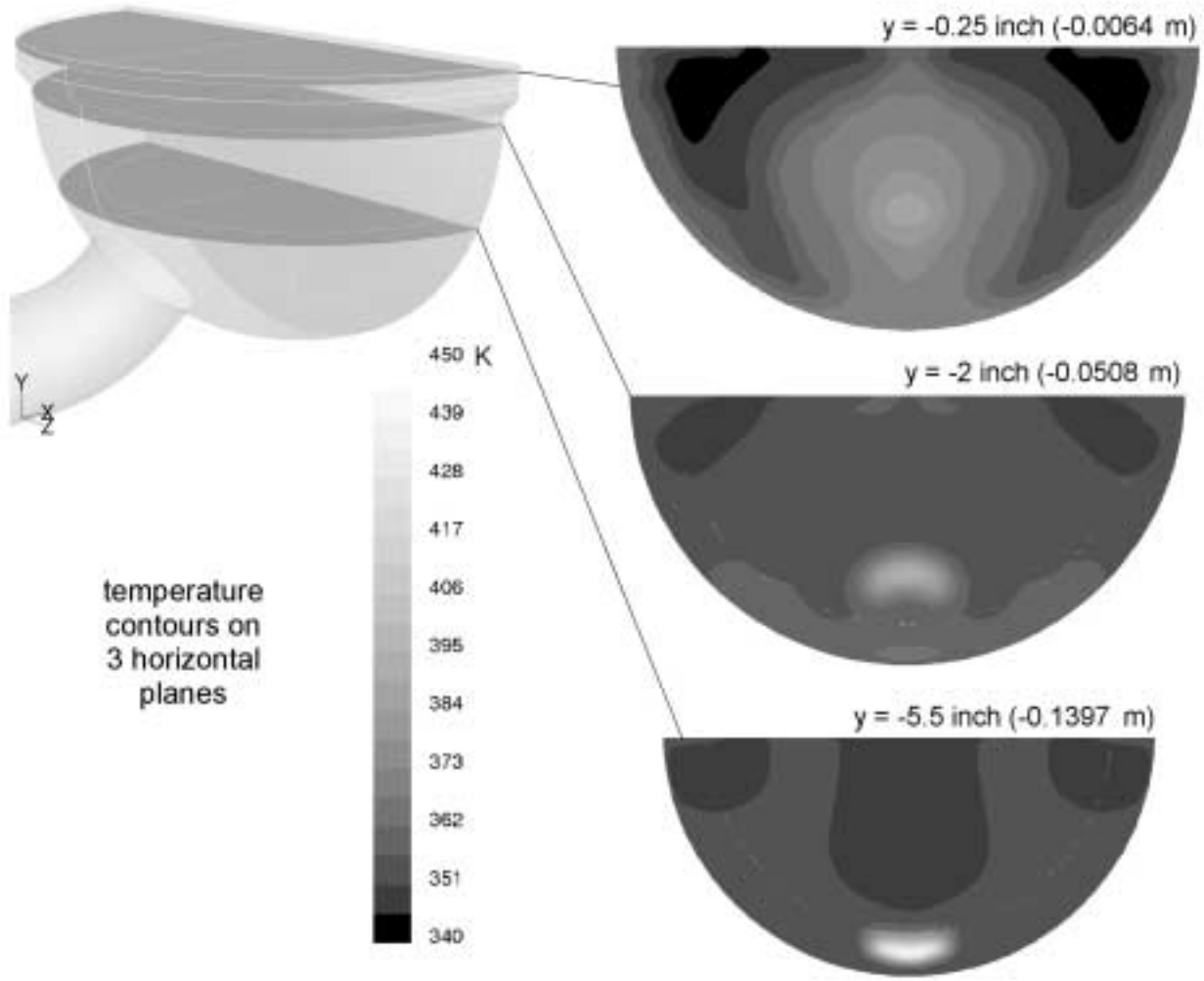

Figure 11. Temperature Contours on Horizontal Planes in Inlet Plenum

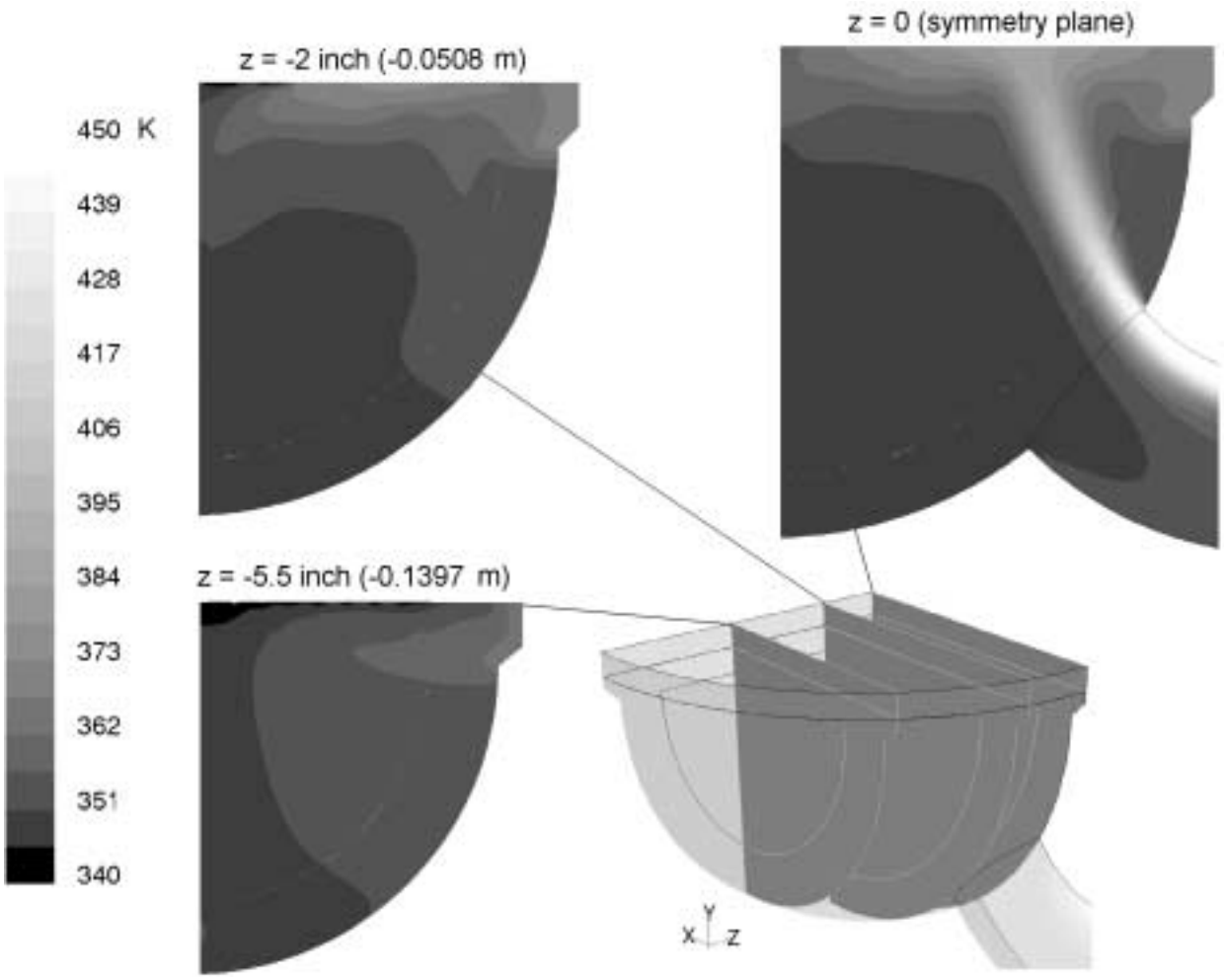

Figure 12. Temperature Contours on Vertical Planes Parallel to Symmetry Plane

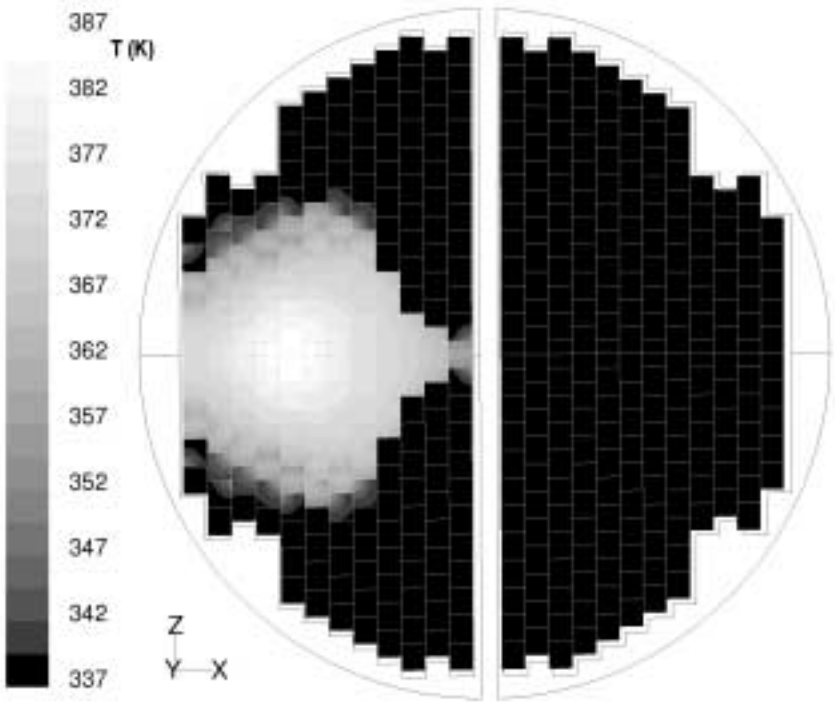

Figure 13. Temperature Contours on Horizontal Plane 1 Inch Above Tube Sheet Entrance

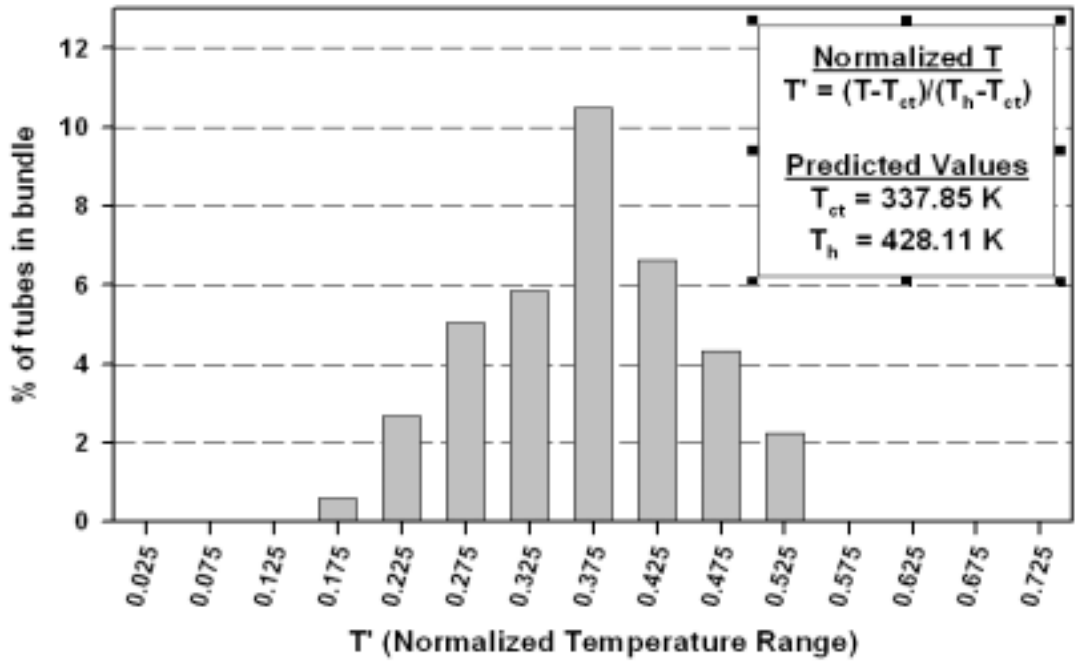

Figure 14. Histogram of Normalized Hot Temperatures 1 Inch Above Tube Sheet Entrance

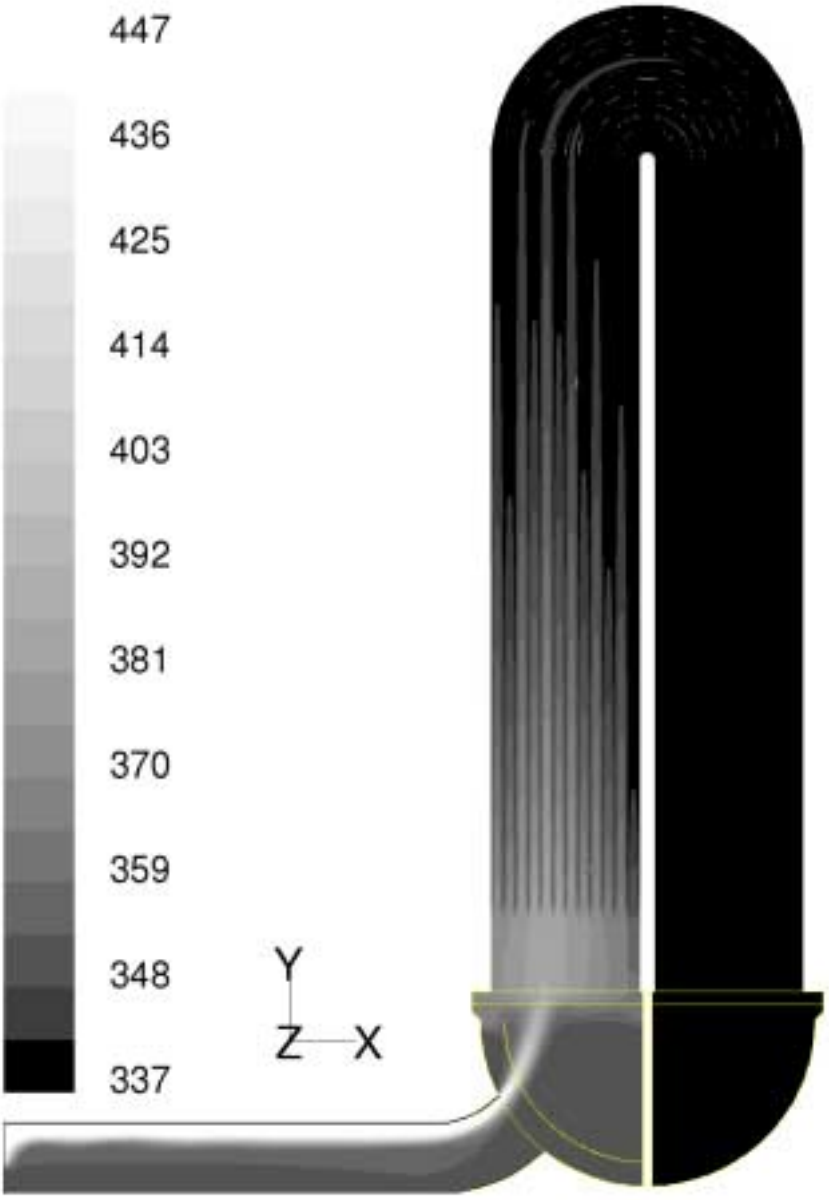

Figure 15. Predicted Temperature Contours on Model Symmetry Plane

Table 1. SF_6 Properties (2.07 Mpa, 300 psia)

T (K)	density (kg/m^3)	T (K)	Cp (J/kg-K)	T (K)	k (W/m-K)	T (K)	viscosity (Pa-s)
333.3	132.9	333.2	832.3	313	.016522	312	1.79 e-05
347.2	122.7	355.4	822.3	323	.017041	472	2.35 e-05
361.1	114.9	377.6	826.9	330	.016781		
388.9	102.7	444.3	864.6	353	.018598		
416.7	94.3			393	.020414		
444.4	86.9			473	.024220		

Table 2. Summary of Boundary Conditions

Input Boundary Condition	SG-S3
Fluid	SF_6, 300 psia
Inlet Velocity (m/s)	0.1045
Inlet Temperature (K)	447.45
Secondary Side Temperature (K)	337.85
Heat Loss Region	Tubes Only

Table 3. **Assumptions and Limitations**

Assumptions	Notes/Limitations
porous tube model	The model is developed to reproduce mass flow and heat loss characteristics of bundle. Velocity is atypical due to an increased flow area. Return flow velocity is low. The impact of the different return velocity has not been assessed. Heat transfer is augmented by increasing the thermal conductivity within the tubes to make up for the increased cross section. Isotropic thermal conductivity also affects conduction in flow direction.
grid density sufficiency	A rigorous grid sensitivity study is not attempted.
inlet boundary conditions	Boundary conditions are determined to match the mass and energy balance from the limited data available. No direct velocity measurements are available and a single temperature measurement provides the mass averaged temperature.
adiabatic plenum divider plate	The steel plate separating the inlet and outlet plenums is assumed adiabatic. A limited sensitivity study, not documented in this report, suggests that the heat loss across this plate is only 1% of the total tube bundle heat loss.
adiabatic tube sheet	The nearly 4-inch thick steel tube sheet, which supports the tubes and separates the cooling water from the hot inlet plenum, is assumed to be adiabatic. The effect of this assumption is not assessed.
all tubes receive to the same cooling	No information is given about the secondary side cooling of the tubes other than an inlet and outlet temperature, a calculated mass flow rate, and a few measurements of temperature in the tubes at the top of the bundle. Tubes in the center of the bundle may or may not be cooled as effectively as tubes on the exterior of the bundle. The CFD model assumes each tube is subjected to the same conditions at all locations. Heat transfer is a significant governing parameter. The implications of this simplification have not been assessed.
symmetry model	This assumption could limit the potential physical oscillations of the buoyant plume in the inlet plenum.

Table 4. Comparison of Test Data (SG-S3) with FLUENT Predictions

Parameter	Westinghouse 1/7th Test Data*	FLUENT Prediction	Difference
Heat Loss at Tubes (kW)	3.56	3.69	3.7 %
# Hot Tubes	75	82	7 tubes (3.2%)
# Cold Tubes	141	134	-7 tubes
T_h Hot Leg (average Hot T (^oC))	159.3	155	-4.3 ^oC
T_c Hot Leg (average Cold T (^oC))	86.8	80.1	-6.7 ^oC
m Hot Leg (mass flux (kg/s))	.06	.0586	-2.3 %
T_{ht} Tubes (average Hot T (^oC))	100.8	100	-0.8 ^oC
T_{ct} Tubes (average Cold T (^oC))	64.7	64.7	0
m_t Tubes (mass flux (kg/s))	0.12	0.1206	0.5 %
m_t/m (recirculation ratio)	2.01	2.06	2.5 %
f (mixing fraction^2)	0.85	0.81	-4.7 %

* Permission to use this EPRI Licensed Material is granted by EPRI.

Table 5. Boundary Conditions for Sensitivity Studies

Sensitivity Study	hot leg inlet temperature T_{in} (K)	hot leg inlet velocity V_{in} (m/s)	turbulence model	tube entrance pressure drop coefficient	tube flow viscous loss coefficients (1/m; $1/m^2$)	bundle heat transfer coefficient (W/m^2K)
Base Case	447.45	0.1045	RSM	45.06	(137.9; 9.09E+09)	250
Inlet Temperature reduced by 15 K	**432.45**	-	-	-	-	-
Hot Leg Mass Flow Increased 20%	-	**0.1254**	-	-	-	-
Turbulence Model lower order model	-	-	**RNG**	-	-	-
Tube Entrance Pressure Drop increased 25%	-	-	-	**56.325**	-	-
Viscous Tube Loss increased 25%	-	-	-	-	**(172.4; 1.14E+07)**	-
Tube Heat Transfer increased coefficient	-	-	-	-	-	**5000**
Tube Heat Transfer decreased coefficient	-	-	-	-	-	**100**

Table 6. Summary of Sensitivity Study Results

parameter	base case	inlet temperature (-15 deg)	hot leg inlet mass flow (+ 20%)	turbulence model (→ RNG)	tube sheet entrance loss (+25%)	viscous tube flow loss (+25%)	tube heat transfer (h = 5000)	tube heat transfer (h = 100)
heat loss at tubes (kW) (% difference)	**3.69**	**3.21** (-13%)	**4.33** (+17.3%)	**3.85** (+4.3%)	**3.69**	**3.58** (-3%)	**3.53** (-4.3%)	**3.85** (4.3%)
# hot tubes (difference)	**82**	**82**	**82**	**82**	**82**	**82**	**88** (+ 6)	**81** (- 1)
$\mathbf{T_h}$ - hot leg (^{o}C) (difference (^{o}C))	**155**	**144.7** (-10.3)	**160.1** (+5.1)	**153** (-2)	**155.2** (+0.2)	**156.4** (+1.4)	**157** (+2)	**153** (-2)
$\mathbf{T_c}$ - hot leg (^{o}C) (difference (^{o}C))	**80.1**	**79.8** (-0.3)	**81.8** (+1.7)	**76.8** (-3.3)	**80.6** (+0.5)	**82.9** (+2.8)	**84** (+3.9)	**76.6** (-3.5)
m - hot leg (kg/s) (% difference)	**0.0586**	**0.0589** (+0.5%)	**0.0653** (11.4%)	**0.0601** (+2.6%)	**0.0585** (-0.2%)	**0.0577** (-1.5%)	**0.0573** (-2.2%)	**0.0598** (+2.0%)
$\mathbf{T_{ht}}$ - tubes (^{o}C) (difference (^{o}C))	**100**	**97.1** (-2.9)	**103.2** (+3.2)	**97.3** (-2.7)	**100.6** (+0.6)	**102.7** (+2.7)	**100.1** (+0.1)	**96.8** (-3.2)
$\mathbf{T_{ct}}$ - tubes (^{o}C)	**64.7**	**64.7**	**64.7**	**64.7**	**64.7**	**64.7**	**64.7**	**64.7**
$\mathbf{m_t}$ - tubes (kg/s) (% difference)	**0.1206**	**0.1135** (-5.9%)	**0.1299** (+7.7%)	**0.1173** (-2.7%)	**0.1191** (-2.2%)	**0.1077** (-10.7%)	**0.1028** (-14.8%)	**0.1433** (+18.8%)
$\mathbf{m_t/m}$ - recirculation ratio (% difference)	**2.06**	**1.93** (-6.3%)	**1.99** (-3.4%)	**1.95** (-5.3%)	**2.04** (-1.0%)	**1.87** (-9.2%)	**1.79** (-13.1%)	**2.4** (+16.5%)
f - mixing fraction[2] (% difference)	**0.81**	**0.82** (+1.2%)	**0.79** (-2.5%)	**0.91** (+12.3%)	**0.80** (-1.2%)	**0.81**	**0.93** (+14.8%)	**0.77** (-4.9%)